AMERICAN SOCIETY FOR MICROBIOLOGY | Infection and Immunity

| Microbial Pathogenesis | Full-Length Text

Ehrlichia Notch signaling induction promotes XIAP stability and inhibits apoptosis

LaNisha L. Patterson,[1] Caitlan D. Byerly,[1] Regina Solomon,[1] Nicholas Pittner,[1] Duc Cuong Bui,[1] Jignesh Patel,[1] Jere W. McBride[1,2,3,4,5]

AUTHOR AFFILIATIONS See affiliation list on p. 17.

ABSTRACT *Ehrlichia chaffeensis* has evolved multiple strategies to evade innate defenses of the mononuclear phagocyte. Recently, we reported the *E. chaffeensis* tandem repeat protein (TRP)120 effector functions as a Notch ligand mimetic and a ubiquitin ligase that degrades the nuclear tumor suppressor, F-box and WD repeat domain-containing 7, a negative regulator of Notch. The Notch intracellular domain (NICD) is known to inhibit apoptosis primarily by interacting with X-linked inhibitor of apoptosis protein (XIAP) to prevent degradation. In this study, we determined that *E. chaffeensis* activation of Notch signaling increases XIAP levels, thereby inhibiting apoptosis through both the intrinsic and executioner pathways. Increased NICD and XIAP levels were detected during *E. chaffeensis* infection and after TRP120 Notch ligand mimetic peptide treatment. Conversely, XIAP levels were reduced in the presence of Notch inhibitor DAPT. Cytoplasmic and nuclear colocalization of NICD and XIAP was observed during infection and a direct interaction was confirmed by co-immunoprecipitation. Procaspase levels increased temporally during infection, consistent with increased XIAP levels; however, knockdown (KD) of XIAP during infection significantly increased apoptosis and Caspase-3, -7, and -9 levels. Furthermore, treatment with SM-164, a second mitochondrial activator of caspases (Smac/DIABLO) antagonist, resulted in decreased procaspase levels and increased caspase activation, induced apoptosis, and significantly decreased infection. In addition, RNAi KD of XIAP also decreased infection and significantly increased apoptosis. Moreover, ectopic expression of TRP120 HECT Ub ligase catalytically defective mutant in HeLa cells decreased NICD and XIAP levels and increased caspase activation compared to HeLa cells with functional HECT Ub ligase catalytic activity (TRP120-WT). This investigation reveals a mechanism whereby *E. chaffeensis* modulates Notch signaling to stabilize XIAP and inhibit apoptosis.

KEYWORDS XIAP, *Ehrlichia chaffeensis*, apoptosis, Notch signaling, caspase

Ehrlichia chaffeensis is an obligately intracellular gram-negative bacterium and the etiologic agent of human monocytotropic ehrlichiosis, a life-threatening emerging tick-borne zoonosis (1). *E. chaffeensis* preferentially infects mononuclear phagocytes and has evolved sophisticated molecular-based strategies to evade host defense mechanisms for survival (2–18). Immune evasion strategies of *E. chaffeensis* are mediated, in part, by tandem repeat protein (TRP) effectors that elicit strong host antibody responses during infection and are secreted by the type 1 secretion system (T1SS) (19–22). Notably, TRP120 decorates the surface of dense-cored ehrlichia and has multiple moonlighting functions including acting as a transcription factor, HECT E3 ubiquitin ligase, and cellular signaling ligand mimic to repurpose or modulate host cell signaling (2, 9, 13–16, 18, 23). These TRP120 functions directly impact host gene expression and chromatin epigenetics, pathogen–host interactions, and cellular signaling (2, 4–7, 9, 12–14, 18, 24, 25).

Two apoptosis pathways, extrinsic and intrinsic, have been defined and are well characterized. The extrinsic pathway is activated through a death ligand receptor

Editor Craig R. Roy, Yale University School of Medicine, New Haven, Connecticut, USA

Address correspondence to Jere W. McBride, jemcbrid@utmb.edu.

The authors declare no conflict of interest.

See the funding table on p. 17.

Received 3 January 2023
Accepted 7 June 2023
Published 18 August 2023

resulting in the activation of Caspase-8 and induction of the execution pathway leading to apoptosis (26–28). In comparison, the intrinsic pathway is initiated by various nonreceptor-mediated stimuli that result in mitochondrial changes, specifically mitochondrial permeability transition (MPT). MPT results in cytochrome c release, triggering the formation of a complex known as an apoptosome and subsequent Caspase-9 activation resulting in apoptosis (29, 30). Execution of apoptosis occurs when Caspase-8 and/or -9 cleave inactivated executioner Caspase-3/7 into active forms, leading to the cleavage of various downstream targets important for cell survival (29, 31, 32). Modulation of several genes that regulate host apoptotic mitochondrial events (intrinsic apoptosis) occurs during *E. chaffeensis* infection including Bcl-2, BirC3, and downregulation of apoptotic inducers, such as Bik, BNIP3L, and hematopoietic cell kinase (HCK) (33). The *E. chaffeensis* effector, ECH0825, is known to inhibit Bax-induced apoptosis by increasing mitochondrial manganese superoxide dismutase (MnSOD) to reduce reactive oxygen species-mediated damage (25). Although the manipulation of intrinsic apoptosis as a survival mechanism for *E. chaffeensis* has been previously reported, there remain significant unanswered questions about the mechanisms involved.

Our laboratory has recently reported that *E. chaffeensis* evasion of monocyte host defenses involves activation of conserved host signaling pathways, including Wnt, Notch, and Hedgehog (2, 13, 14). Notably, TRP120 activates the evolutionarily conserved Notch signaling pathway using a novel molecularly defined pathogen-encoded Notch SLiM ligand mimic found within the tandem repeat (TR) domain (13). Notch signaling plays significant roles in cellular homeostasis, MHC Class II expression, B- and T-cell development, and modulation of innate immune mechanisms such as autophagy and apoptosis (34–39). Recently, we have reported that *E. chaffeensis* TRP120-induced Notch signaling results in downregulation of toll-like receptor (TLR) 2/4 expression (5). Moreover, we determined that TRP120 degrades the Notch negative regulator, F-box and WD repeat domain-containing 7 (FBW7), resulting in increased levels of several oncoproteins, including the Notch intracellular domain (NICD), which regulates cell survival and apoptosis (15). Therefore, *E. chaffeensis* induced Notch signaling, and increased levels of NICD during *E. chaffeensis* infection may play an important role in inhibiting apoptosis.

Caspases are the enzymes primarily responsible for mediating apoptosis (26, 29, 40), and apoptosis can be blocked by inhibiting caspase activity. The X-linked inhibitor of apoptosis protein (XIAP) is the most potent inhibitor of apoptosis (IAP) (41, 42). XIAP directly binds and inhibits initiator and executioner caspases, including Caspases-9 and -3, respectively (42–46). Interestingly, Lui et al. demonstrated that NICD suppresses host cell apoptosis by increasing XIAP stability (47). NICD and XIAP interaction prevents ubiquitination and degradation of XIAP, thereby inhibiting apoptosis. Moreover, Caspase-3 and -8 are known to cleave XIAP into two fragments [Baculovirus IAP Repeat (BIR) 1–2 and BIR3-RING], leading to differential inhibition of extrinsic and intrinsic apoptotic pathways (48). BIR3-RING fragments are potent inhibitors of Caspase-9, resulting in inhibition of Bax-mediated (intrinsic) apoptosis. Therefore, Notch activation and FBW7 degradation during *E. chaffeensis* infection may stabilize XIAP as a mechanism to inhibit intrinsic, caspase-dependent apoptosis.

In this study, we reveal a novel mechanism whereby *E. chaffeensis* inhibits apoptosis through Notch activation resulting in NICD stabilization of XIAP. Inhibition of apoptosis through modulation of Notch signaling provides further evidence that *E. chaffeensis* hijacks evolutionarily conserved signaling pathways to evade innate host defense mechanisms.

RESULTS

E. chaffeensis infection and TRP120 increases XIAP levels

We recently demonstrated that NICD levels temporally increase during *E. chaffeensis* infection (15). Increased levels of NICD were associated with TRP120 ubiquitination and degradation of a Notch negative regulator, FBW7. NICD is known to directly

bind the XIAP BIR-RING domain and prevent XIAP autoubiquitination and degradation (47), thereby inhibiting apoptosis. To investigate potential XIAP upregulation during infection, THP-1 cells were incubated with *E. chaffeensis* [multiplicity of infection (MOI) 50], and XIAP protein and transcription levels were analyzed by immunoblot and qPCR. Levels of XIAP were unchanged in uninfected THP-1 cells (Fig. 1A). In comparison, increases in XIAP protein levels were demonstrated over the course of infection, with significant increases detected at 24, 48, and 72 h post-infection (hpi) (Fig. 1A). Interestingly, additional cleaved fragment was observed at 48 and 72 hpi and identified as the BIR3-RING domain of XIAP (Fig. 1A) (48). When cleaved, BIR3-RING also acts as a potent inhibitor of the intrinsic apoptotic pathway by binding the Caspase-9 monomer preventing its cleavage and heterodimerization (48). Moreover, transcriptional levels of XIAP were also shown to be significantly upregulated in a temporal manner (Fig. 1B). XIAP expression was evaluated in THP-1 cells treated with recombinant TRP120 TR (rTRP120-TR) domain, or the recently described TRP120 Notch ligand memetic SLiM (TRP120-TR-P6) peptide (13). A significant temporal increase in XIAP levels was detected in cells treated with rTRP120-TR or TRP120-TR-P6 peptide (Fig. 1C and E) compared to rTRX or TRP120-TR-P5-treated cells (Fig. 1D and F), demonstrating *E. chaffeensis* TRP120 promotes increased XIAP levels.

NICD interacts with XIAP during infection

To determine whether NICD directly binds XIAP during infection, confocal microscopy was performed to visualize XIAP/NICD colocalization. Interestingly, strong NICD and XIAP colocalization according to Mander's coefficient (MC) was observed in *E. chaffeen-*

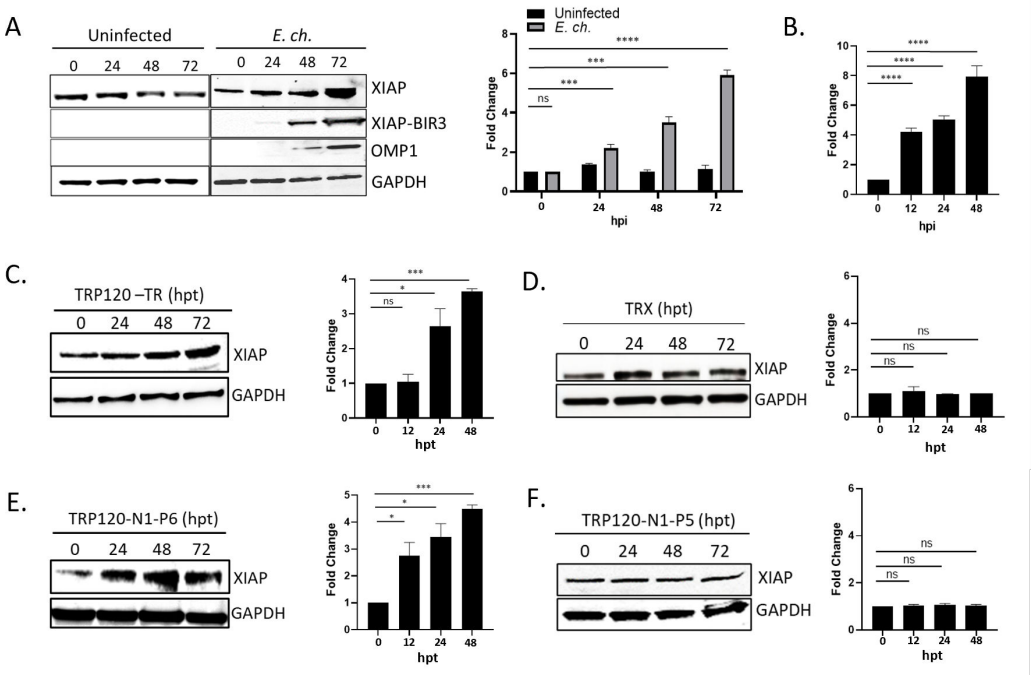

FIG 1 XIAP levels increase during *E. chaffeensis* infection. (A) Immunoblot of XIAP, cleaved XIAP-BIR3, and outer membrane protein-1 (OMP-1) expression normalized to glyceraldehyde 3-phosphate dehydrogenase (GAPDH) in uninfected and *E. chaffeensis*-infected THP-1 cells at 0–72 hpi (MOI 50). The major OMP-1 is used to confirm infection. Fold differences in XIAP levels in *E. chaffeensis*-infected and uninfected THP-1 cells. (B) Changes in XIAP transcript levels in *E. chaffeensis*-infected and uninfected THP-1 cells (0 hpi) as determined by RT-qPCR analysis. (C) Immunoblot and quantification of XIAP in TRP120-TR-treated THP-1 cells (2 µg/mL; 2 h). (D) Immunoblot and quantification of XIAP in TRP120-N1-P6 memetic peptide-treated THP-1 cells (1 µg/mL; 2 h). Bar graphs represent mean ± SD. ns (not significant), $P > 0.05$, * $P < 0.05$, *** $P < 0.001$, **** $P < 0.0001$. Experiments were performed in triplicate ($n = 3$) and representative images are shown.

sis-infected cells at 24 (MC = 0.9), 48 (MC = 0.9), and 72 (MC = 0.8) hpi (Fig. 2A). XIAP levels were also temporally increased at 24, 48, and 72 hpi based on mean fluorescence intensity (Fig. 2B). By immunoblot, significant temporal increases in XIAP and NICD were detected (Fig. 2C). Co-immunoprecipitation (Co-IP) of XIAP and NICD from uninfected and *E. chaffeensis*-infected lysates (24 hpi) demonstrated direct interaction and increased XIAP and NICD levels (Fig. 2D).

Notch activation and XIAP stabilization by NICD

To confirm that the increase in XIAP levels was a direct result of Notch activation, THP-1 cells were pretreated with DAPT (5 µg/mL; 1 h), a Notch γ-secretase inhibitor. Cells pretreated with DAPT inhibitor and infected with *E. chaffeensis* (MOI 50) exhibited decreased XIAP levels at 24 and 48 hpi (Fig. 3A). Similar results were also shown with SAHM1 treatment, which prevents assembly of the active Notch transcriptional complex (Fig. S1). To further determine the direct relationship between NICD and XIAP levels during *E. chaffeensis* infection, uninfected and *E. chaffeensis*-infected THP-1 cells were pretreated alone or in combination with DAPT (5 µg/mL; 1 h) and SM-164 (100 nM; 12 h), a second mitochondrial activator of caspases (Smac/DIABLO) mimetic compound that antagonizes IAPs to promote activation of caspases and apoptosis (45). DAPT/SM-164 pretreatment was given prior to induction of cell death by tumor necrosis factor alpha (TNF-α; 100 ng/mL; 12 h), followed by subsequent infection with *E. chaffeensis* (MOI 50).

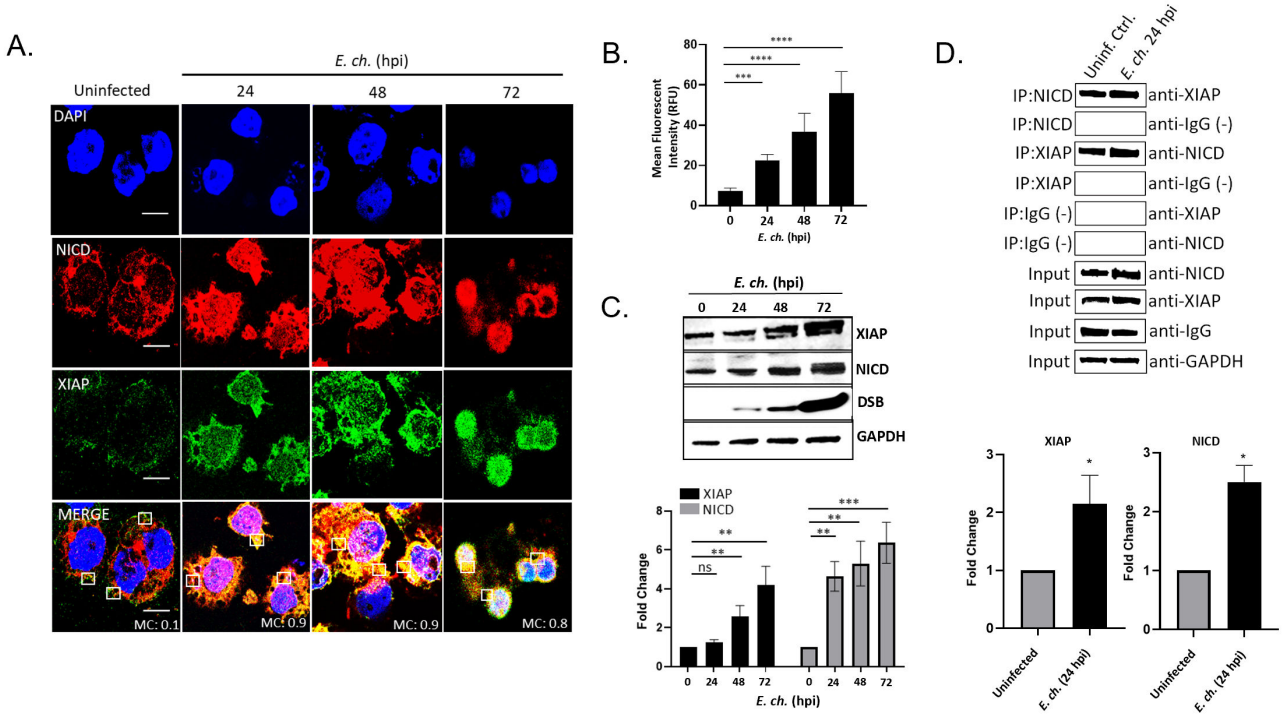

FIG 2 NICD interaction with XIAP during *E. chaffeensis* infection. (A) Uninfected or *E. chaffeensis*-infected THP-1 cells at 0, 24, 48, and 72 hpi (MOI 50) were probed for endogenous NICD (red) or endogenous XIAP (green) and colocalization visualized by immunofluorescent confocal microscopy (scale bar = 10 µm). Colocalization was quantitated by MC (0 no colocalization; +1 strong colocalization). Mean fluorescence intensity of the XIAP protein expression in THP-1 cells (n = 20). Mean pixel values were obtained using the ImageJ Measure Analysis tool. Background intensity was determined and subtracted from the fluorescence intensity value of the cells. The mean value from each group was an average of 20 cells. (C) Immunoblot and fold differences of XIAP or NICD normalized to glyceraldehyde 3-phosphate dehydrogenase (GAPDH) in *E. chaffeensis*-infected cells at 0–72 hpi (MOI 50). (D) Co-IP was performed to examine the direct interaction between XIAP and NICD at 24 hpi compared to the IgG-negative control. Western blot analysis was normalized to GAPDH expression. NICD and XIAP levels were measured from the Co-IP. Quantification of NICD or XIAP levels from one representative Co-IP experiment is shown. ns (not significant), $P > 0.05$, * $P < 0.05$, ** $P < 0.01$, *** $P < 0.001$, **** $P < 0.0001$. Experiments were performed in triplicate (n = 3) and representative images are shown.

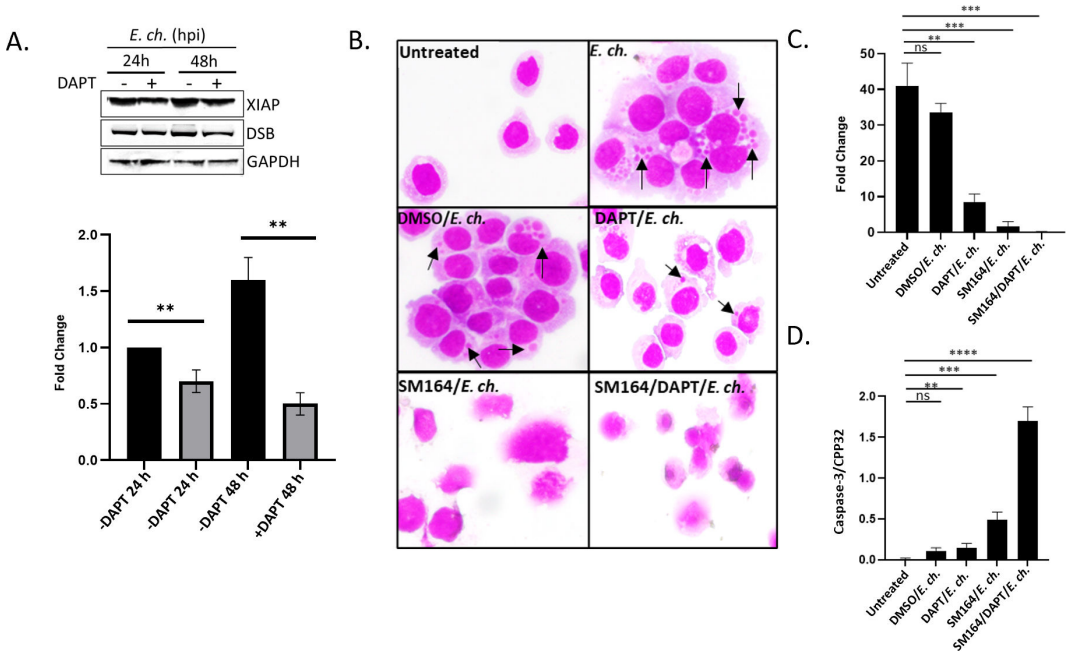

FIG 3 Notch activation stabilizes XIAP during *E. chaffeensis* infection. (A) Immunoblot and differences (fold change) of XIAP expression normalized to glyceraldehyde 3-phosphate dehydrogenase (GAPDH) in *E. chaffeensis*-infected THP-1 cells with or without DAPT pretreatment at 24 or 48 hpi. Cells were infected with *E. chaffeensis* after DAPT (5 µg/mL; 1 h) pretreatment. XIAP protein levels were determined at 24 and 48 hpi by Western blot analysis and fold-change differences of XIAP levels were determined. (B) H&E stained uninfected or *E. chaffeensis*-infected THP-1 cells untreated or pretreated with vehicle (DMSO) or SM164 (100 nM; 12 h) alone or in combination with DAPT (5 µg/mL; 1 h). Cell death was stimulated by TNF-α (100 ng/mL; 12 h) post-treatment and prior to the addition of *E. chaffeensis* (MOI 50). Black arrows identify *E. chaffeensis* morulae. (C) Fold-change difference in *dsb* transcript levels in cells depicted in Fig. 3B. (D) Quantification of Caspase-3/CPP32 activity determined at an absorbance of 405 nm. Bar graphs represent mean ± SD. ns (not significant), ** $P < 0.01$, *** $P < 0.001$, **** $P < 0.0001$. Experiments were performed in triplicate and representative images are shown.

A 22% reduction in cell viability was observed by trypan blue exclusion in uninfected THP-1 cells treated with TNF-α alone (Fig. S2). Hematoxylin and eosin (H&E) staining of THP-1 cells treated with DAPT/SM-164 did not contain morulae, displayed significant cell death, and had significantly decreased ehrlichial infection compared to uninfected, *E. chaffeensis*-infected, dimethyl sulfoxide (DMSO) alone, or with DAPT or SM-164 alone treated cells (Fig. 3B and C).

To further confirm Notch signaling promotes cell survival and ehrlichial infection, Caspase-3/CPP32 activity was determined by measuring the absorbance of DEVD-pNA, a Caspase-3 substrate (49). An increase in Caspase-3/CPP32 levels (~2 fold) was detected in THP-1 cells treated with both DAPT and SM-164 compared to uninfected, DMSO treated, or *E. chaffeensis*-infected cells treated with either DAPT or SM-164 (Fig. 3D). Significant upregulation of Caspase-3/CPP32 activity was also demonstrated in the SM-164-treated cells compared to untreated cells; however, DAPT/SM-164 combination treatment demonstrated significantly higher Caspase-3/CPP32 levels (Fig. 3D). Collectively, these data suggest that XIAP is stabilized by NICD during *E. chaffeensis* infection.

XIAP is required for antiapoptotic activity and increased infection

The effect of XIAP on *E. chaffeensis* infection was examined using small interfering RNA (siRNA) knockdown (KD) of XIAP in THP-1 cells. siRNA KD of XIAP resulted in a 77% KD efficiency (Fig. 4A). *E. chaffeensis* infection was significantly decreased in XIAP-KD cells (24 hpi) compared to scrambled control siRNA-treated cells (Fig. 4B and C). To determine whether the decrease in ehrlichial load was caused by the induction of apoptosis due to XIAP destabilization, cell viability was determined by flow cytometry with the Muse Count & Viability Kit. XIAP-KD cells exhibited a viability of ~8% compared

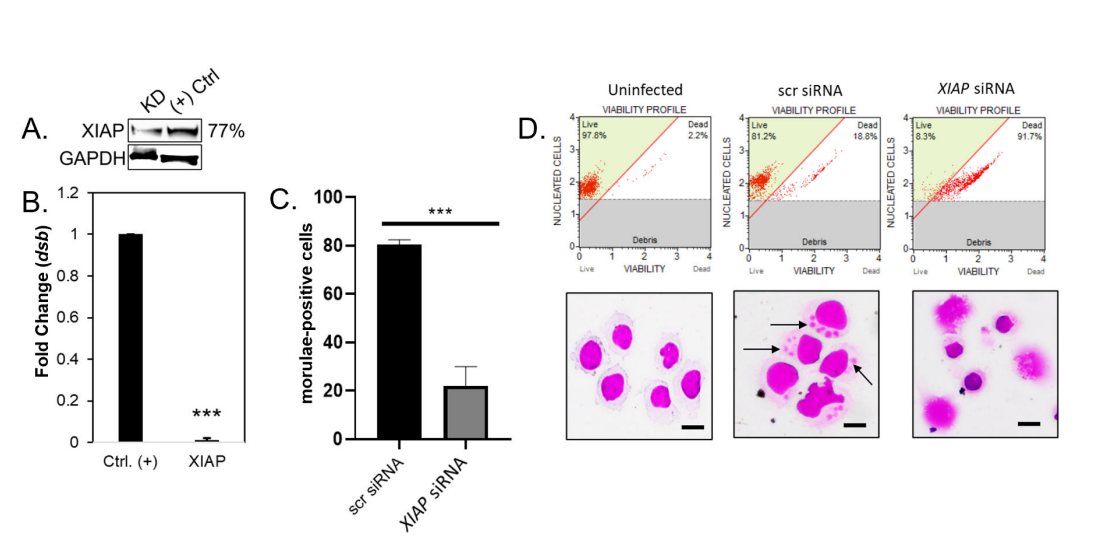

FIG 4 XIAP enhances cell viability to promote *E. chaffeensis* infection. (A) Immunoblot depicting KD efficiency of *XIAP* in siRNA KD cells compared to scr siRNA control from *E. chaffeensis* THP-1 cells harvested at 24 hpi. Percent KD of XIAP relative to positive control is shown in the right panel. glyceraldehyde 3-phosphate dehydrogenase (GAPDH) was utilized as a loading control. (B) siRNA-transfected THP-1 cells were infected with *E. chaffeensis* (MOI 100, 24 hpi). Scrambled siRNA (scrRNA) was used as a negative control. *E. chaffeensis* infection was quantified (fold change) at 24 hpi and was determined by qPCR amplification of the *dsb* gene. KDs were performed with at least three biological and technical replicates for *t*-test analysis. (C) Quantification of morulae-positive cells in scr or *XIAP* siRNA-treated THP-1 cells by H&E staining. (D) Representative image of H&E stained uninfected or *E. chaffeensis*-infected scr or *XIAP* siRNA-treated cells (arrows identify *E. chaffeensis* morulae). Quantitative analysis of cell viability by the Muse Count & Viability Kit for uninfected or *E. chaffeensis*-infected scr or *XIAP* siRNA-treated cells is shown. Bar graphs represent mean ± SD. ***$P < 0.001$. Experiments were performed in triplicate and representative images are shown.

to 81% in scr-KD cells (Fig. 4D). Furthermore, XIAP-KD cells displayed morphological changes associated with apoptosis including shrinkage of the cell, fragmentation into membrane-bound apoptotic bodies, and nuclear fragmentation (Fig. 4D).

XIAP inhibits apoptosis during *E. chaffeensis* infection

Smac/DIABLO is a cytosolic antagonist of IAPs (50). To determine the significance of IAPs during *E. chaffeensis* infection, THP-1 cells were pretreated with SM-164 (100 nM; 12 h), a Smac/DIABLO mimetic compound. Cell death was induced by TNF-α (100 ng/mL; 12 h), followed by subsequent infection with *E. chaffeensis*. Treatment with SM-164 resulted in a significant reduction in ehrlichial infection as determined by confocal microscopy and qPCR of the *dsb* gene (Fig. 5A and B). Importantly, cells treated in combination with SM-164/TNF-α had 10–20% viability and exhibited morphological changes in apoptosis including membrane blebbing, nuclear fragmentation, and cell shrinkage (Fig. 5A and C; Fig. S3A). In comparison, untreated or DMSO-treated cells had cell viability ranging from 82% to 92% and 63% to 82%, respectively, with lower viability of DMSO-treated cells due to the addition of TNF-α (Fig. 5C; Fig. S3A). In addition, there were unremarkable morphological changes associated with untreated or DMSO-treated cells (Fig. 5A). These data further suggest that NICD stabilization of XIAP results in antiapoptotic activity during *E. chaffeensis* infection. In addition, an increase in early and late apoptotic cells was shown in SM-164/TNF-α-treated cells compared to untreated, DMSO or either SM-164 or DMSO/TNF-α-treated cells. Importantly, preincubation of THP-1 cells with Caspase-9 inhibitor, Z-LEHD-FMK TFA (20 µM; 2 h), prior to SM-164/TNF-α treatment reversed apoptotic effects demonstrated with SM-164/TNF-α (Fig. 5A through C; Fig. S3A through C). Collectively, these data demonstrate that increases in XIAP levels inhibit apoptosis during *E. chaffeensis* infection.

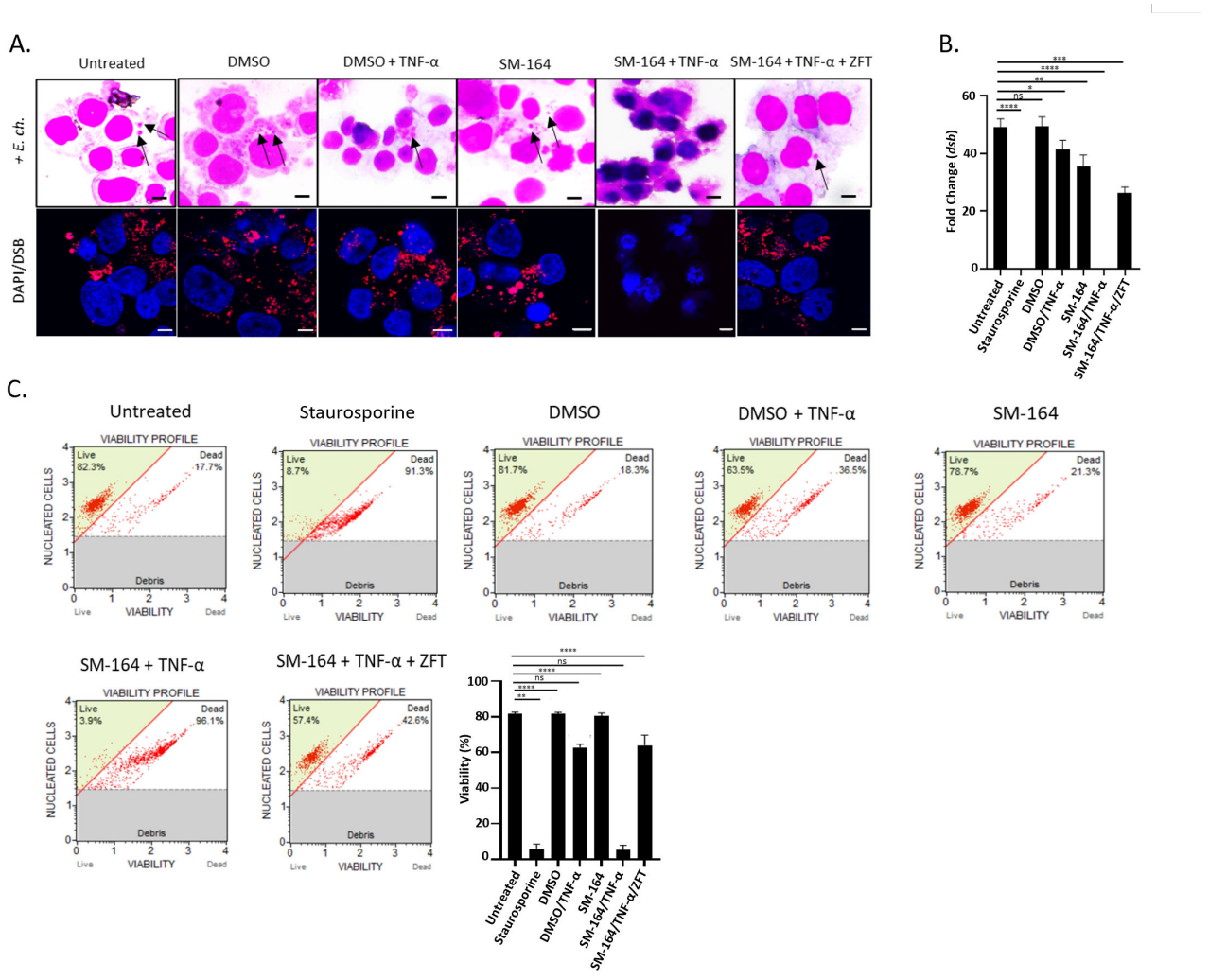

FIG 5 XIAP stabilizes pro-caspase levels to inhibit apoptosis. *E. chaffeensis*-infected THP-1 cells (MOI 50) were pretreated with vehicle (DMSO) or SM-164 alone (100 nM; 12 h) or in combination with Caspase-9 inhibitor, Z-LEHD-FMK TFA (20 µM; 2 h). Cell death was stimulated with TNF-α (100 ng/mL; 12 h) or staurosporine (100 ng/mL; 12 h, positive apoptosis control) post-treatment and prior to the addition of *E. chaffeensis* (MOI 50). (A) The presence of *E. chaffeensis* determined by H&E staining (black arrows) and immunofluorescent confocal microscopy. Infected THP-1 cells were probed with anti-disulfide bond formation protein (DSB) and tetramethylrhodamine isothiocyanate conjugate (red) to confirm the presence of morulae by immunofluorescent confocal microscopy. Nuclei were stained with 4′,6′-diamidino-2-phenylindole DAPI (blue). Apoptotic cells were identified by visualization of nuclear morphology by DAPI (bar = 10 µm). (B) Fold change difference of *dsb* transcript levels in the indicated cell samples. (C) Cell viability was determined using the Muse Count & Viability Kit and quantification of cell viability percentage in the previously mentioned treatment groups is shown. Bar graphs represent mean ± SD. ns (not significant), $P > 0.05$, * $P < 0.05$, ** $P < 0.01$, *** $P < 0.001$, **** $P < 0.0001$. Experiments were performed in triplicate and representative images are shown.

Pro-Caspase levels during *E. chaffeensis* infection

Studies have demonstrated that XIAP differentially inhibits caspases through its BIR domains (48). The BIR2 domain directly binds apoptotic executioner Caspase-3 and -7 using a two-site interaction mechanism for inhibition of apoptosis (51). XIAP also sequesters Caspase-9 in a monomeric state using the BIR3 domain, preventing the catalytic activity of Caspase-9 (45). Therefore, XIAP is directly associated with inhibition of downstream caspases. During *E. chaffeensis* infection, temporal levels of Caspase-3, -7, and -9 increased during infection (Fig. 6A). Temporal increases in Caspase-3, -7, and -9 gene transcription were also detected during *E. chaffeensis* infection (Fig. S4).

To demonstrate that XIAP was directly associated with downstream caspase inhibition, THP-1 cells were pretreated with SM-164 (100 nM; 12 h) and TNF-α

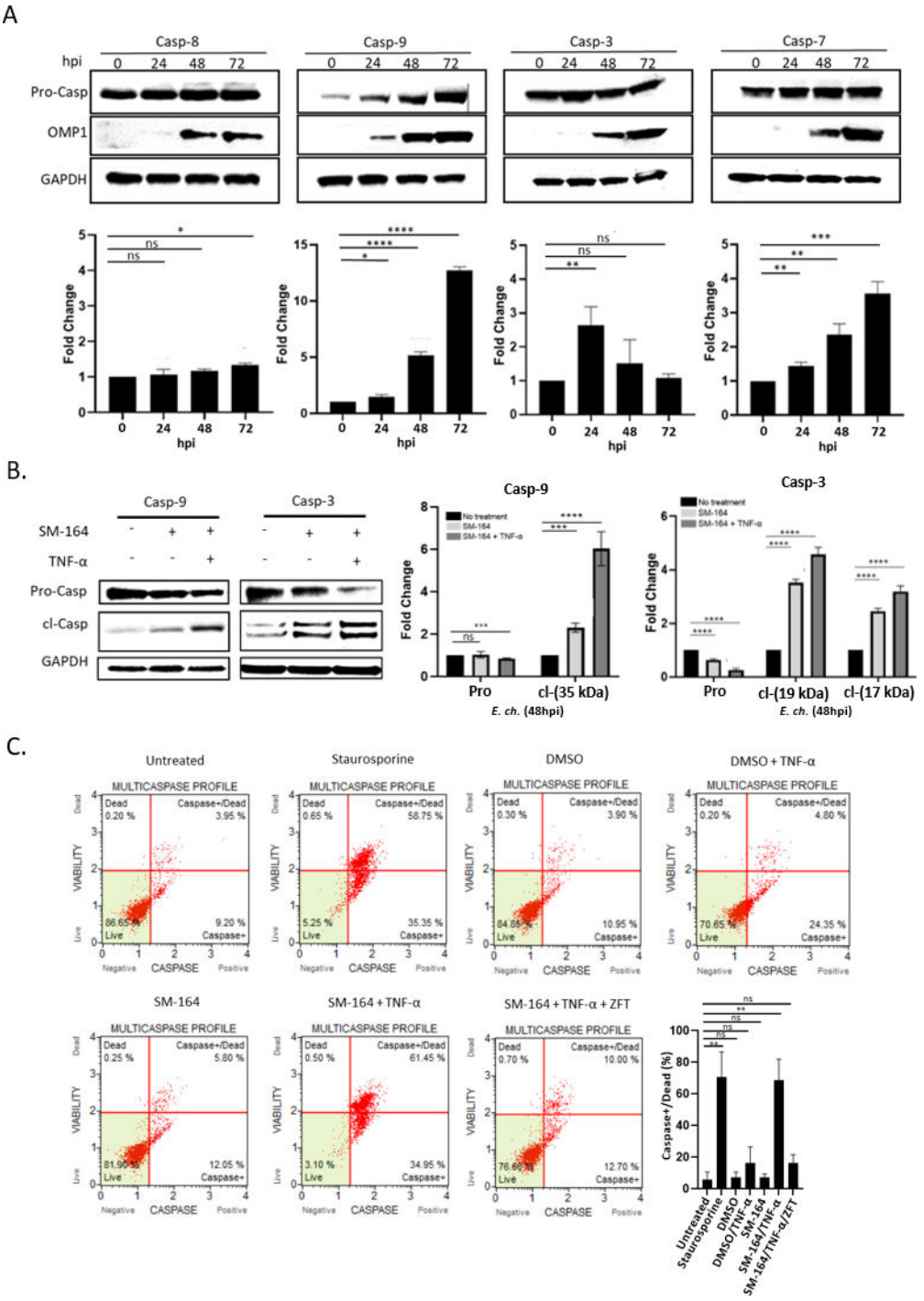

FIG 6 XIAP stabilizes pro-caspase levels to inhibit apoptosis during *E. chaffeensis* infection. (A) Immunoblots and differences (fold change) in pro-Casp-8, -9, -3, and -7 in *E. chaffeensis*-infected cells at 0, 24, 48, and 72 hpi. Pro-caspase levels were normalized to glyceraldehyde 3-phosphate dehydrogenase (GAPDH). Outer membrane protein 1 (OMP-1) is a major outer membrane protein used to confirm infection. GAPDH is utilized as a loading control. (B) Immunoblot and quantification of the fold change of *E. chaffeensis*-infected cells untreated or pretreated with SM-164 alone (100 nM; 12 h) or in combination with TNF-α (100 ng/mL; 12 h). TNF-α treatment was administered after SM-164 treatment and prior to the addition of *E. chaffeensis* (MOI 50). Cells were probed for total and cleaved Caspase-3 or -9 and differences (fold change) are shown. (C) *E. chaffeensis*-infected THP-1 cells were pretreated with vehicle (DMSO) or SM-164 alone (100 nM; 12 h) or SM-164 in

(Continued on next page)

FIG 6 (Continued)

combination with Caspase-9 inhibitor, Z-LEHD-FMK TFA (20 µM; 2 h). Z-LEHD-FMK TFA was administered 1 h prior to SM-164 treatment. Cell death was stimulated with TNF-α (100 ng/mL; 12 h) or staurosporine (100 ng/mL; 12 h; positive apoptosis control) post-treatment and prior to the addition of *E. chaffeensis* (MOI 50) in the indicated samples. Percentages of live, caspase+, caspase+ and dead, total caspase+, and dead cells determined using the Muse MultiCaspase Kit. Quantification of Caspase+/dead cells (%) is shown. Bar graphs represent mean ± SD. ns (not significant), $P > 0.05$, *$P < 0.05$, **$P < 0.01$, ***$P < 0.001$, ****, $P < 0.0001$. Experiments were performed in triplicate and representative images are shown.

(100 ng/mL; 12 h), infected with *E. chaffeensis* infection (MOI 50) and Caspase-9 and -3 levels were determined. The SM-164/TNF-α-treated cells had significantly lower levels of pro-Caspase-9 and -3, and significantly increased levels of cleaved (active) Caspase-9 and -3 (Fig. 6B). To demonstrate that XIAP was directly associated with downstream caspase inhibition, THP-1 cells were treated with SM-164 in combination with TNF-α, infected with *E. chaffeensis* infection (MOI 50) and multi-caspase levels were determined by flow cytometry. A significant increase in the percentage of caspase+/dead cells with SM-164/TNF-α treatment was detected (Fig. 6C). These data demonstrate increased XIAP levels inhibit caspase activation and apoptosis during *E. chaffeensis* infection.

FBW7 ubiquitination and proteasomal degradation stabilizes XIAP

We have recently demonstrated FBW7 degradation during *E. chaffeensis* infection results in increased levels of FBW7 regulated oncoproteins including NICD, phosphorylated c-Jun, MCL-1, and cMYC (15). Data demonstrated that TRP120 ubiquitination of FBW7 results in FBW7 degradation, enhancing infection. To determine the effect of FBW7 and NICD on XIAP and Caspase-3 and Caspase-9 activation, HeLa cells were transfected with catalytically inactive TRP120 (TRP120-C520S) and treated with TRP120-N1-P6 Notch memetic peptide (1 µg/mL) for 2 h to activate Notch signaling followed by induction of cell death by TNF-α (100 ng/mL; 12 h). HeLa cells ectopically expressing TRP120-C520S displayed increased cleaved Caspases-3 and -9 compared to uninfected or TRP120-WT-transfected cells (Fig. 7A). TRP120-C520S-expressing cells displayed decreased XIAP levels in comparison to TRP120-WT-expressing cells (Fig. 7B). Collectively, these data demonstrate that TRP120 FBW7 degradation stabilizes NICD for subsequent increased XIAP expression and inhibition of caspase activation during *E. chaffeensis* infection.

DISCUSSION

Inhibition of host cell apoptosis is an important survival strategy utilized by *E. chaffeensis* (33, 52, 53). Previous studies have demonstrated that the T4SS effector protein, ECH0825, inhibits host cell apoptosis in human monocytes (54). ECH0825 localizes to mitochondria and inhibits Bax-induced apoptosis by increasing mitochondrial MnSOD and reducing reactive oxygen species-mediated damage (54). Furthermore, upregulation of apoptotic inhibitor genes during *E. chaffeensis* infection, including BCL-2 and BIRC3, and downregulation of apoptotic inducers, such as BIK, BNIP3L, and hematopoietic cell kinase have also been reported (33). However, there is little information related to *E. chaffeensis* modulation of caspase activation. In this study, we have identified a mechanism by which *E. chaffeensis* TRP120 effector activates the Notch signaling pathway to inhibit caspase-dependent apoptosis through NICD and XIAP interaction.

We recently identified a TRP120 Notch SLiM ligand memetic motif responsible for Notch activation during *E. chaffeensis* infection (13). In addition, we demonstrated that *E. chaffeensis* and rTRP120 activate Notch signaling to downregulate TLR 2/4 expression for intracellular survival (5). TRP120 Notch activation was recently confirmed to occur through a TRP120 TR Notch SLiM ligand mimic that directly binds to the Notch receptor in a region containing the known ligand binding region (13). Although a Notch SLiM mimic has been recently identified, its role in *E. chaffeensis* survival has not been fully elucidated. In this study, we investigated the functional implications of TRP120 Notch SLiM mimic activation of Notch signaling during *E. chaffeensis* infection. A novel antiapoptotic mechanism involving IAP proteins potently inhibiting the catalytic activity

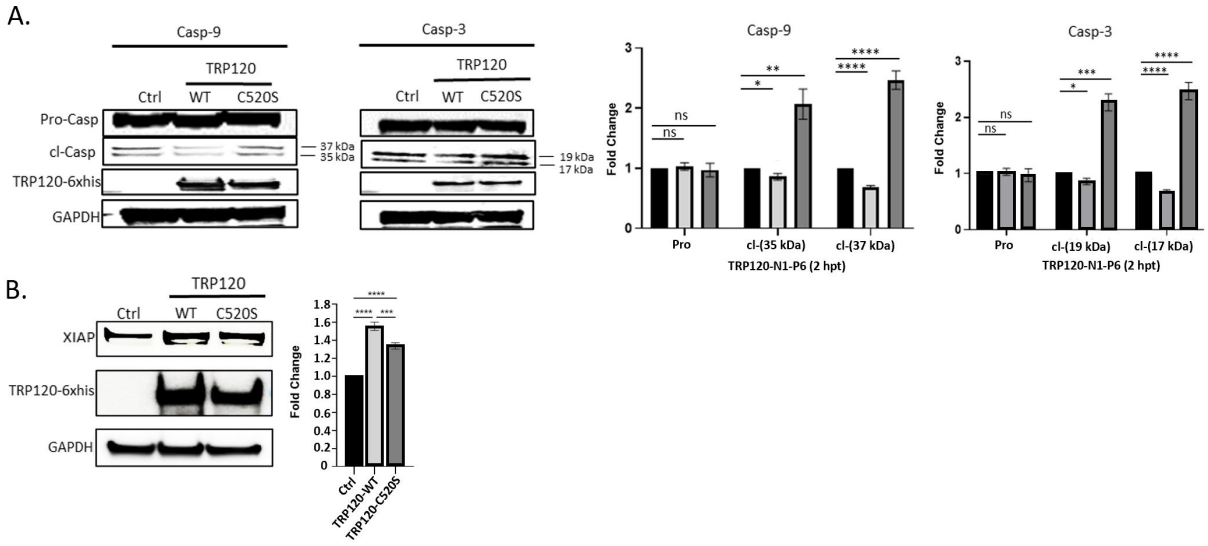

FIG 7 FBW7 degradation during *E. chaffeensis* infection enhances XIAP stability and caspase activation. HeLa cells were transfected with empty vector, TRP120-WT or catalytic-inactive TRP120 (TRP120-C520S) for 24 h, stimulated with TRP120-N1-P6 memetic peptide to activate Notch signaling (1 ug/mL; 2 h) and cell death was subsequently induced by TNF-α (100 ng/mL; 48 h). (A) Immunoblot of Pro- and cleaved Caspase-3 or −9 in vector, TRP120-WT or TRP120-C520S-treated cells. Changes in pro- and cleaved Caspase-3 or -9 levels in TRP120-WT or TRP120-C520S-treated cells compared with empty vector are shown. (B) Immunoblot of XIAP in vector, TRP120-WT or TRP120-C520S-treated cells. Change in XIAP levels in TRP120-WT or TRP120-C520S-treated cells compared with empty vector are shown. Caspase and XIAP levels were normalized to glyceraldehyde 3-phosphate dehydrogenase (GAPDH). Bar graphs represent mean ± SD. ns (not significant), $P > 0.05$, *$P < 0.05$, **$P < 0.01$, ***$P < 0.001$, ****$P < 0.0001$. Experiments were performed in triplicate ($n = 3$) and representative images are shown.

of caspases through regulation of Notch signaling was defined and is illustrated in the graphical abstract (Fig. 8).

Pathogens have evolved various means of subverting innate immune defense of the host for survival (2, 43, 55–60). One of the most well-studied mechanisms of bacterial pathogens is targeting intracellular signal transduction cascades. Pathways such as MAPK and NF-κB are manipulated by various pathogens (39, 61–63). Manipulation of these innate immune and inflammatory pathways is regulated through bacterial effector proteins and host–pathogen interactions (3, 64). In addition, inhibition of apoptosis is well documented as a mechanism used by bacteria and viruses to subvert innate immune defense (2, 56, 62, 65, 66). Although intracellular bacterial pathogens manipulate apoptosis by various mechanisms, exploitation of the Notch signaling pathway is a strategy that has not been reported.

The Notch signaling pathway is an evolutionarily conserved cell signaling pathway in Metazoans (67, 68). The Notch pathway is known to play critical roles in cellular homeostasis, differentiation, and cell proliferation (68). Recently, evidence has demonstrated Notch signaling to also play roles in innate immunity and inflammation, including regulation of TLR expression, inflammatory cytokines, macrophage activation, MHC class II expression, B- and T-cell development, autophagy, and apoptosis (37, 69–73). Interestingly, Notch signaling is activated in macrophages by lipopolysaccharide (LPS) (74), *Mycobacterium bovis* Bacillus Calmette–Guérin (BCG) (75), and as we recently reported, *E. chaffeensis* (5). Activation of Notch by LPS and by *M. bovis* BCG is associated with the regulation of cytokine signaling through different mechanisms. The expression of canonical Notch ligand, Jagged-1, is induced by LPS in a JNK-dependent manner (74). In comparison, *M. bovis* BCG was shown to upregulate Notch-1 and activate the Notch-1 signaling pathway, leading to the expression of SOCS3, a negative regulator of cytokine signaling (75). In comparison, *E. chaffeensis* has been demonstrated to activate Notch signaling through a Notch SLiM ligand mimic found within the TR domain of the TRP120 effector resulting in downregulation of TLR 2/4 (5, 13).

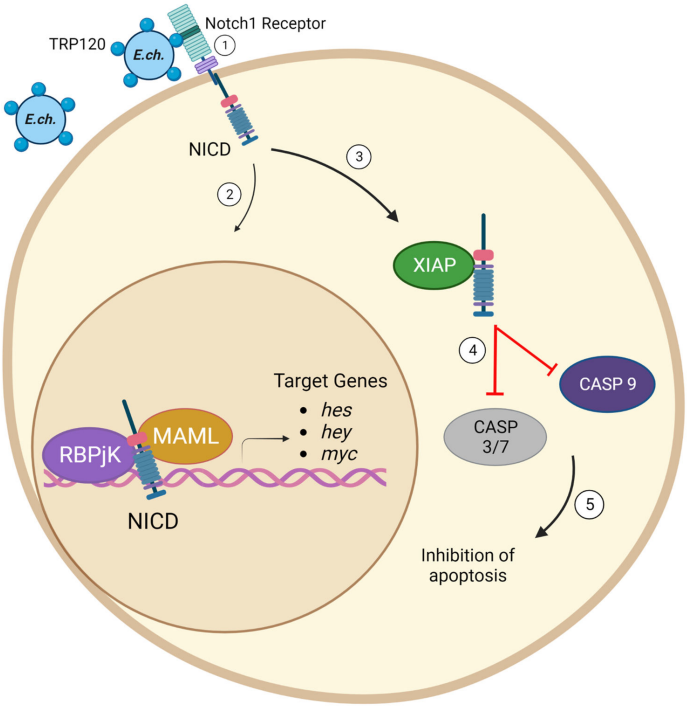

FIG 8 Graphical abstract of *E. chaffeensis* TRP120 Notch-mediated apoptosis inhibition. Infectious dense-cored *E. chaffeensis* with theTRP120 T1SS effector localized to the bacterial surface binds (1) to the ligand binding region (LBR) of the Notch-1 receptor via the Notch SLiM ligand mimic (13) and activates Notch signaling (2). NICD translocates to the nucleus and activates Notch gene transcription and (3) directly binds XIAP to prevent XIAP degradation (4, 5), inhibiting Caspase-3, -7, and -9 activation and apoptosis.

Interestingly, Notch has been shown to inhibit apoptosis by directly interfering with the ubiquitination of the most potent inhibitor of apoptosis, XIAP (47). NICD directly binds the BIR3-RING domain of XIAP to inhibit autoubiquitination. Inhibition of XIAP autoubiquitination results in stabilization of XIAP levels, leading to inhibition of apoptosis (47). In this study, we demonstrated increases in XIAP expression over the course of *E. chaffeensis* infection. A cleavage product was observed at later time points which correlated with the XIAP BIR3-RING domain. Studies have demonstrated this domain to be a potent inhibitor of the intrinsic apoptotic pathway through direct binding to Caspase-9 (48). XIAP sequesters Caspase-9 in a monomeric state, which serves to prevent catalytic activity (76). Previous studies have demonstrated that *E. chaffeensis* inhibits apoptosis through the intrinsic apoptotic pathway by blocking the BCL-2 pathway (33). In addition, we have recently demonstrated that engagement of the BCL-2 antiapoptotic cellular programming during *E. chaffeensis* infection is caused by activation of the Hedgehog signaling pathway (2). Induction of BCL-2 resulted in inhibition of Caspase-3 and -9, preventing activation of intrinsic apoptosis (2). Therefore, evidence supports the inhibition of intrinsic apoptosis as a survival mechanism for *E. chaffeensis*. Importantly, both rTRP120 and the TRP120 Notch SLiM ligand memetic peptide upregulated XIAP expression in a time-dependent manner, with significant upregulation occurring at later time points, as demonstrated with *E. chaffeensis*-infected cells. These data support the role of the TRP120 induced Notch signaling activation leading to increased XIAP levels.

NICD and XIAP levels increased simultaneously and temporally. We have previously determined that NICD levels increase during infection, attributed in part to *E. chaffeensis* TRP120 ubiquitinating and degrading the Notch negative regulator, FBW7 (15). Here, we demonstrate NICD to both colocalize and directly bind with XIAP at later time points of *E. chaffeensis* infection. Interestingly, colocalization of NICD and XIAP occurred in both the cytoplasm and the nucleus during *E. chaffeensis* infection. Selective localization of pro-caspases in different subcellular compartments has been previously demonstrated (77). Pro-caspase and active Caspase-3, -7, and -9 are mainly found in the cytosolic fraction; however, Caspase-3 and -9 are also found in the mitochondrial fraction, while Caspase-7 is also found in the microsomal fraction in untreated Jurkat T lymphocytes (77). Caspase-3 is the only major caspase found in the nucleus (77). XIAP expression has been found to be mainly cytoplasmic; however, it is also present in the nucleus in specific cell types. XIAP nuclear translocation has been previously associated with aberrant cell division and anchorage-independent growth (78, 79). Previous data have demonstrated that increases in XIAP are not associated with stimulation of XIAP transcription by NICD (47). Therefore, further investigation is needed to determine the functional implications of NICD/XIAP colocalization in the nucleus during *E. chaffeensis* infection (47). Inhibition of Notch activation by DAPT, a γ-secretase inhibitor, reversed increases in XIAP levels during *E. chaffeensis* infection. DAPT inhibits Notch receptor enzymatic hydrolysis, NICD release, and downstream transcriptional activation by inhibiting γ-secretase activity. Hence, inhibition of NICD is directly associated with decreases in XIAP levels.

Apoptosis is an important innate defense mechanism against microbial infection; however, various intracellular pathogens hijack apoptosis by inhibiting either extrinsic or intrinsic apoptosis through different mechanisms (2, 80–82). We demonstrated the importance of XIAP expression in inhibition of apoptosis during *E. chaffeensis* infection. siRNA KD of XIAP significantly reduced *E. chaffeensis* infection. This finding was associated with apoptosis, as demonstrated by Muse Count & Viability Assays and microscopy demonstrating cellular morphological hallmarks of apoptosis. siRNA-treated cells showed significant cell blebbing, shrinkage of the cell, and nuclear fragmentation. XIAP siRNA-treated cells contained a significant reduction in morulae compared to scrambled siRNA (scrRNA) cells. Interestingly, *Anaplasma phagocytophilum* also appears to inhibit apoptosis by preventing XIAP degradation (43). Cleaved fragments of XIAP were not detected in *A. phagocytophilum*-infected neutrophils (43), suggesting that XIAP degradation is blocked during *A. phagocytophilum* infection. In contrast, we detected an increase in XIAP cleavage product (30 kDa), which we identified as XIAP BIR3-RING. As previously stated, the XIAP BIR3-RING cleavage product has been shown to strongly inhibit intrinsic apoptosis. Differences in the presence of the cleavage product observed between *E. chaffeensis* and *A. phagocytophilum* are not well understood and need further investigation. These findings indicate that modulating IAPs to inhibit apoptosis may be a conserved mechanism utilized by various intracellular bacterial pathogens for survival.

Various studies have demonstrated XIAP as the most potent endogenous inhibitor of caspases due to weaker binding and inhibition of caspases by other IAP proteins. Interestingly, XIAP has been shown to inhibit both the executioner and intrinsic apoptotic pathways using various domains found within its structure. XIAP inhibits the executioner pathway by directly binding to Caspase-3 and -7 through the linker region between the BIR1 and BIR2 domains (51). As previously mentioned, XIAP also directly binds to Caspase-9 via the BIR3 domain (45, 46, 76). We have demonstrated levels of pro-Caspase-3,-7, and -9 temporally increase during *E. chaffeensis* infection. However, there were only minor changes in Caspase-8 levels during infection, demonstrating that mitochondrial-mediated apoptosis is the predominantly targeted for inhibition. In comparison, inhibition of Caspase-8 activation and Bid cleavage has been demonstrated in *A. phagocytophilum*-infected human neutrophils (43).

Previous data have shown that transcriptional levels of caspases do not change at earlier timepoints during *E. chaffeensis* infection (83). In comparison, our data show transcriptional regulation at 12 hpi. Pro-Caspase-3 transcript and protein levels increased

at 24 hpi but protein levels decreased at 48 and 72 hpi. Cleavage of pro-Caspase-3 levels coincides with BIR3-RING cleavage products observed at 48 and 72 hpi. Activated Caspase-3 has previously been demonstrated to cleave XIAP (48), resulting in BIR1-2 and BIR3-RING fragments. The BIR1-2 fragment inhibits Caspase-3 and -7; however, BIR1-2 is a less potent IAP than full-length XIAP and may also be susceptible to further degradation (84). In comparison, the BIR3-RING fragment blocks activation of Caspase-9 by directly binding to and inhibiting activity (45, 46, 76). Therefore, activation of Caspase-3 may lead to XIAP BIR3-RING fragments that inhibit intrinsic apoptosis through direct Caspase-9 binding; however, more studies are needed to fully elucidate this mechanism. Interestingly, similar evidence of inhibition of Caspase-3 and -9 activation during *A. phagocytophilum* infection has been reported where activation of Caspase-3 and -9 was linked to inhibition of XIAP degradation (43).

Inhibition of caspase activation by XIAP is mediated by the endogenous IAP inhibitor, SMAC/Diablo. During induction of apoptosis, SMAC/Diablo is processed and released from the mitochondria where it binds to the BIR2 and BIR3 domains of XIAP to antagonize XIAP activity (45, 50). SM-164 is a bivalent, SMAC mimetic that induces apoptosis (85). Treatment with SM-164 in the presence of TNF-α significantly reduced cell viability and ehrlichial load. An increase in caspase-positive apoptotic cells was shown with SM164/TNF-α treatment. Importantly, SM-164/TNF-α-treated cells pre-treated with Caspase-9 inhibitor, Z-LEHD-FMK TFA, blocked full induction of apoptosis during *E. chaffeensis* infection. TNF-α has been demonstrated to inhibit apoptosis through both the extrinsic and intrinsic apoptotic pathways. Activation of the extrinsic pathway results in the cleavage of cytosolic BID to truncated p15 BID (tBID), which translocates to mitochondria and triggers cytochrome c release (86). Therefore, reversal of cell death by Caspase-9 inhibitor, Z-LEHD-FMK TFA, may occur through BID activation. In addition, SM-164 treatment resulted in decreased pro-caspase and increased levels of cleaved Caspase-9 and -3 during infection. These results demonstrate direct correlation of XIAP activity and caspase inhibition during *E. chaffeensis* infection. Previous studies have shown that the reduction in XIAP either does not occur or takes place at later time points in various cancer cell models, several hours after robust apoptosis induction, suggesting that the degradation of XIAP is not required for apoptosis induction by Smac mimetics (45, 85, 87). Therefore, in our model, induction of apoptosis is dependent on the activity of XIAP on caspase inhibition alone, rather than XIAP degradation.

During *E. chaffeensis* infection, TRP120 ubiquitinates Notch negative regulator, FBW7, resulting in degradation (15). Degradation of FBW7 is known to result in increased NICD levels (88). HeLa cells transfected with TRP120-C520S catalytic mutant displayed an increase in cleaved Caspase-3 and -9, and a decrease in XIAP levels, demonstrating a direct relationship between FBW7 stabilization of NICD levels and subsequent increased XIAP expression and caspase inhibition. Collectively, this study serves to provide insight into the molecular details of how TRP120 Notch signaling leads to increased XIAP expression through direct interaction with NICD, leading to inhibition of caspase activation and apoptosis for *E. chaffeensis* survival.

There are multiple questions that remain to be answered regarding *E. chaffeensis* regulation of apoptosis. IAP proteins have been previously shown to interact with one another to form IAP-IAP complexes that inhibit apoptosis (89). Many of the IAP-IAP complexes consist of one or more of four key IAPs: c-IAP1, c-IAP2, XIAP, and survivin. Whether XIAP functions in a complex with other IAPs to inhibit apoptosis during *E. chaffeensis* infection remains unknown. Evolutionarily conserved signaling pathways, such as Notch and Hedgehog, play key roles in regulation of apoptosis (35, 90, 91). TRP120 has been demonstrated to inhibit apoptosis by activation of Hedgehog signaling (2). Further investigation is needed to understand potential crosstalk between Notch, Hedgehog, and potentially other signaling pathways that are activated during *E. chaffeensis* infection and associated with apoptosis regulation.

In conclusion, we demonstrated *E. chaffeensis* Notch activation results in an XIAP-mediated antiapoptotic program. Our findings reveal an *E. chaffeensis* initiated, Notch

signaling regulated, antiapoptotic mechanism involving IAP proteins that inhibit caspase activation (Fig. 8). This study gives further insight into the molecular mechanisms used by obligate intracellular pathogens to exploit conserved signaling pathways to suppress innate defenses and promote infection.

MATERIALS AND METHODS

Cell culture and *E. chaffeensis* infection

Human monocytic leukemia cells (THP-1; ATCC TIB-202) were maintained in RPMI medium (ATCC) supplemented with 2 mM L-glutamine, 10 mM HEPES, 1 mM sodium pyruvate, 4,500 mg/L glucose, 1,500 mg/L sodium bicarbonate, supplemented with 10% fetal bovine serum (FBS; Invitrogen) at 37°C in 5% CO_2 atmosphere. *E. chaffeensis* (Arkansas strain) was propagated in THP-1 cells. Host cell-free *E. chaffeensis* was prepared as previously described (13). The purified ehrlichia were resuspended in fresh RPMI medium and utilized as needed. For transfection, human cervical epithelial adenocarcinoma cells (HeLa; ATCC CCL-2) were propagated in Dulbecco's modified Eagle's medium (DMEM; Invitrogen, Carlsbad, CA) supplemented with 10% FBS (HyClone, Logan, UT).

Antibodies and reagents

Primary antibodies used in this study for immunofluorescence microscopy and immunoblot analysis include polyclonal rabbit (2042S, Cell Signaling Technology, Danvers MA) or mouse monoclonal α-XIAP (sc-55550, Santa Cruz Biotechnology, Dallas TX), rabbit monoclonal α-Caspase-3 (9662S; Cell Signaling Technology), rabbit monoclonal α-Caspase-7 (9494S; Cell Signaling Technology), rabbit monoclonal α-Caspase-8 (4790T; Cell Signaling Technology), rabbit α-Caspase-9 (9502S; Cell Signaling Technology), polyclonal rabbit α-Notch1 intracellular domain (07-1231; Millipore Sigma, Billerica, MA, USA), rabbit α-TRP120-I1, rabbit monoclonal α-glyceraldehyde 3-phosphate dehydrogenase (GAPDH) (2118L; Cell Signaling Technology), and human monoclonal α-outer membrane protein 1 (92). Synthetic peptides used in this study were commercially generated (Genscript, Piscataway, NJ, USA). The pharmacological inhibitors of XIAP, Notch, and Caspase-9 in this study were SM-164 (56003S; Cell Signaling Technology), DAPT (GSI-IX) (S2215; Tocris Bioscience, Bristol, UK), and Z-LEHD-FMK TFA (S731303; Tocris Bioscience), respectively. Cell death inducers in this study included rhTNF-α (210-TA/CF; R&D Systems, Minneapolis MN) and Staurosporine (9953S; Cell Signaling Technology).

Immunoblot analysis

Cells were infected or treated as indicated in text and figure legends and subsequently lysed with Triton-X 100 supplemented with protease inhibitor cocktail, Halt phosphatase, and phenylmethylsulfonyl fluoride for 30 min, with lysing by pipetting every 10 min on ice. Lysates were cleared by centrifugation at 14,000 × *g* (4°C) for 20 min. Protein concentration of cleared lysates was determined by bicinchoninic acid assay. Laemelli buffer was added to lysates then boiled for 5 min at 95°C. Lysates were then subjected to SDS-PAGE and transferred to nitrocellulose membrane. Membranes were blocked using 5% nonfat milk in Tris-buffered saline with 0.1% Tween 20 (TBST) and then exposed to α-XIAP, α-NICD, α-Casp-3,-7, or -9 or α-GAPDH antibodies overnight at 4°C. Membranes were washed thrice in Tris-buffered saline containing 1% Triton for a total of 30 min followed by 1 h of incubation with horseradish peroxidase-conjugated antirabbit or antimouse secondary antibodies (SeraCare, Milford, MA, USA) (diluted 1:10,000 in 1% nonfat milk in TBST). Proteins were visualized with ECL using a ChemiDoc It^2 imager (UVP) and densitometry performed with VisionWorks software (ver. 8.1). All blots are presented in their original form but may have loss of resolution due to the image compression from the dock system, Chemidoc-it2 Imager.

Quantitative PCR

Uninfected, *E. chaffeensis*-infected or inhibitor-treated THP-1 cells were collected at 0-, 12-, 24-, and 48-h intervals. RNeasy Mini Kit (Qiagen, Valencia, CA, USA) was used to purify RNA followed by cDNA synthesis (0.5 µg of RNA) using iScript RT kit (Bio-Rad) and qPCR was performed using the Brilliant II SYBR Green QPCR master mix (Agilent). PCR primer sequences included *XIAP* (F: 5′-GAGAAGATGACTTTTAACAGTTTGA-3′; R: 5′-TTTTTTGCTTGAAAGTAATGACTGTGT-3′), *CASP-3* (F: 5′-TGCAGCAAACCTCAGGGAAA-3′; R: 5′-AGTAACCCCTGCTTAATCGTCA-3′), *CASP-7* (F: 5′-ATTTAGGCTTGCCGAGGGAC-3′; R: 5′-ATGCTTGGCAGACAATGGAC-3′), *CASP-9* (F: 5′-GGCTGCTCCTGTTGGATGTA-3′; R: 5′-CCTTTTACCCTTGGTTTGGGC-3′), *DSB* (F: 5′-GCTGCTCCACCAATAAATGTATCCT-3′; 5′-gtttcattagccaagaattccgacact-3′), and *GAPDH* (F: 5′-ggagtccactggcgtcttcac-3′; R: 5′-gaggcattgctgatgatcttgag-3′). Relative gene expression was calculated by determining the cycle threshold (Ct) value and normalizing to *GAPDH* as previously described (13).

Co-IP

Magna ChIP™ A/G Chromatin Immunoprecipitation kit (MilliporeSigma, Burlington, MA, USA) was used to investigate XIAP and NICD interactions during *E. chaffeensis* infection. Briefly, THP-1 cells were infected with *E. chaffeensis* (MOI 100) or left uninfected (control) for 24 h. Cells were harvested, and Co-IP was performed, according to the manufacturer's protocol. XIAP and NICD antibodies (Cell Signaling Technology) were used to determine interactions. IgG purified from normal serum was used as control antibody. Bound antigen was eluted, solubilized in 4x SDS sample loading buffer, and processed for immunoblot analysis. The membrane was probed with XIAP or NICD antibody to confirm pulldown. Co-IP was performed in triplicate experiments.

Transfection

HeLa cells (1×10^6) were seeded in a 60 mm culture dish 24 h prior to transfection. All proteins were expressed in a pcDNA3.1+C-6His vector. TRP120 full-length (pcDNA3.1+TRP120_FL_C-6His) and its HECT Ub ligase catalytic inactive mutant (pcDNA3.1+TRP120_C520S_C-6His) were cloned into the pcDNA3.1+C-6His vector at NheI/XbaI sites. pcDNA3.1+C-6His empty vector was used as a control. All vectors were added to Opti-MEM and Lipofectamine 3000 mixture and incubated for 20 min at 37°C. Lipofectamine/plasmid mixtures were added to HeLa cells and incubated for 4 h at 37°C. The medium was aspirated 4 h post-transfection and fresh medium was added to each plate and incubated for 24 h.

Immunofluorescent confocal microscopy

THP-1 cells (1×10^6) were infected with *E. chaffeensis* (MOI 100) for indicated time intervals at 37°C. Cells were collected and fixed using ice-cold 4% formaldehyde and washed with sterile 1× phosphate-buffered saline (PBS) five times for 5 min. Cell samples were permeabilized and blocked in 0.5% Triton X-100 and 2% bovine serum albumin in PBS for 30 min. Cells were washed with sterile 1× PBS three times for 5 min and probed with XIAP, NICD, or DSB antibodies for 1 h at room temperature. Cells were washed with sterile 1 × PBST (0.1% Tween) three times for 5 min and probed with Alexa Fluor IgG (H + L) or Alexa Fluor IgG (H + L) for 30 min at room temperature, washed three times with sterile 1× PBST, and mounted with ProLong Gold antifade reagent with DAPI (Molecular Probes). Slides were imaged on a Zeiss LSM 880 confocal laser scanning microscopy. Mander's correlation coefficients were generated by ImageJ software to quantify the degree of colocalization between fluorophores.

TRP120 recombinant protein and peptide treatment

Recombinant TRP120 containing the TR or thioredoxin (TRX) was expressed in a pBAD expression vector and purified as previously published (93–95). rTRP120-TR was dialyzed in 1× PBS and tested for bacterial endotoxins using the limulus amebocyte lysate test. TRP120 synthetic peptides were produced commercially (Genscript, Piscataway, NJ, USA). THP-1 cells were treated with 2 µg/mL of rTRP120-TR or TRX, or 1 µg/mL of synthetic TRP120 peptides for 0–72 h time points. Cells were collected post-treatment and immunoblot and qPCR analysis was performed.

RNAi KD

Cells (1.0×10^6) were transfected with ON-TARGETplus SMARTpool XIAP siRNA (3 µL) (Dharmacon, Lafayette, CO, USA) using Lipofectamine 3000 (7.5 µL) (Invitrogen, Waltham, MA, USA), according to the manufacturer's instructions. Scrambled siRNA was utilized as a control in both uninfected and *E. chaffeensis*-infected THP-1 cells. The siRNA and Lipofectamine mixture were added to 250 µL of MEM medium (Invitrogen), incubated for 12 min at room temperature and added to cells in a 6-well plate. KD was assessed by immunoblot analysis as previously described. Cells were knocked down for 24 h and infected with *E. chaffeensis* (MOI 100) for 24 h. Cells were then harvested after 24 hpi. Proliferative/cell death analysis was performed on all KD cells. Ehrlichial load was determined by qPCR of *dsb* gene as previously described (8). All siRNA KDs were performed with triplicate technical and biological replicates and significance was determined using a *t*-test analysis.

Drug treatment and cell death analysis

THP-1 cells were untreated or pretreated with vehicle (DMSO), DAPT (5 µg/mL, 1 h), SM-164 (100 nM, 12 h) alone, or in combination with Z-LEHD-FMK TFA (20 µM, 2 h) and incubated at 37°C, 5% CO_2 for 12 h. Z-LEHD-FMK TFA treatment was administered for 2 h prior to SM-164 treatment. Cell death was induced using TNF-α (100 ng/mL, 12 h) and was administered post-treatment of DMSO, SM-164, and Z-LEHD-FMK TFA. Staurosporine (100 ng/mL) was utilized as a positive apoptosis control and was administered post-treatment of DMSO, SM-164, and Z-LEHD-FMK TFA. Cells were infected with *E. chaffeensis* (MOI 50) following induction of cell death for 48 h. Apoptosis was analyzed utilizing various cell death assays.

1. **Trypan blue exclusion**. Cell samples (20 µL) were collected and mixed with an equal volume of trypan blue. Samples were incubated at room temperature for 2 min and then read using the Nexcelom Cellometer Mini (Nexcelom Bioscience LLC, Lawrence, MA, USA).
2. **Caspase-3/CPP32 Assay Kit**. Caspase-3/CPP32 Assay Kit (Colorimetric) [NBP2-54838] was utilized to assess the activity of Caspase-3, according to the manufacturers' protocol.
3. **H&E**. H&E stain was utilized to assess cell morphological changes associated with cell death. Cells were collected and washed with 1× DPBS. Fresh RPMI media were added to the cell samples and fixed onto slides by cytospin (800 x *g*, 5 min). Cells were then fixed by acetone (1 min) and stained with H&E (1 min/stain). Slides were rinsed with DI water and dried prior to analysis using light microscopy. Images were taken using the Olympus CellSens software.
4. **Guava Muse Cell Analyzer**. Various Muse assays were utilized according to the manufacturers' protocol to determine apoptosis:
    a. The Muse Count & Viability Kit was used to determine cell counts (cells/mL) and viability (%) (Part Number MCH100102).
    b. The Muse MultiCaspase Kit (Part Number: MCH100109) was used to determine caspase activation and cellular plasma membrane permeabiliza-

tion, or cell death. The percentage of live, caspase+, caspase+ and dead, total caspase+, and dead cells was determined.
c. The Muse Annexin V & Dead Cell Kit (Part Number: MCH100105) was used to determine live, early, and late apoptosis and cell death. The percentage of live, early apoptotic, late apoptotic, total apoptotic, and dead cells was determined.

Statistical analysis

All data are represented as the means ± standard deviation of data obtained from at least three independent experiments done with triplicate biological replicates. Experiments performed with technical replicates are indicated in figure legends and the material and methods section. Analyses were performed using a two-way ANOVA or two-tailed Student's *t*-test (GraphPad Prism 6 software, La Jolla, CA, USA). $P < 0.05$ was considered statistically significant.

ACKNOWLEDGMENTS

We thank the Maxim Ivannikov and UTMB Optical Microscopy Core for assistance with confocal microscopy.

This work was supported by the National Institute of Allergy and Infectious Diseases grant AI158422 to J.W.M., James W. McLaughlin Endowment and an NIH 1F31AI152424 predoctoral fellowships to L.L.P., and T32AI007526-20 Biodefense training fellowship to C.D.B.

We declare no conflict of interest.

AUTHOR AFFILIATIONS

[1]Department of Pathology, University of Texas Medical Branch, Galveston, Texas, USA
[2]Department of Microbiology and Immunology, University of Texas Medical Branch, Galveston, Texas, USA
[3]Center for Biodefense and Emerging Infectious Diseases, University of Texas Medical Branch, Galveston, Texas, USA
[4]Sealy Institute for Vaccine Sciences, University of Texas Medical Branch, Galveston, Texas, USA
[5]Institute for Human Infections and Immunity, University of Texas Medical Branch, Galveston, Texas, USA

AUTHOR ORCIDs

LaNisha L. Patterson http://orcid.org/0000-0003-1839-5429
Caitlan D. Byerly http://orcid.org/0000-0002-3448-0669
Jere W. McBride http://orcid.org/0000-0003-3335-1539

FUNDING

Funder	Grant(s)	Author(s)
HHS | NIH | National Institute of Allergy and Infectious Diseases (NIAID)	AI158422	Jere W McBride
HHS | NIH | National Institute of Allergy and Infectious Diseases (NIAID)	AI152424	LaNisha L Patterson
HHS | NIH | National Institute of Allergy and Infectious Diseases (NIAID)	AI007526	Caitlan D Byerly

AUTHOR CONTRIBUTIONS

LaNisha L. Patterson, Conceptualization, Data curation, Formal analysis, Investigation, Methodology, Validation, Visualization, Writing – original draft, Writing – review and editing | Caitlan D. Byerly, Data curation, Methodology | Regina Solomon, Data curation | Nicholas Pittner, Data curation | Duc Cuong Bui, Data curation, Methodology | Jignesh Patel, Data curation, Methodology | Jere W. McBride, Conceptualization, Formal analysis, Funding acquisition, Project administration, Resources, Supervision, Validation, Visualization, Writing – review and editing

ADDITIONAL FILES

The following material is available online.

Supplemental Material

Fig. S1 (IAI00002-23-s0001.tif). SAHM1 treatment decreases XIAP during *E. chaffeensis* infection.
Fig. S2 (IAI00002-23-s0002.tif). TNF-α induces cell death in uninfected THP-1 cells.
Fig. S3 (IAI00002-23-s0003.tif). Inhibition of XIAP enhances apoptosis in *E. chaffeensis*-infected cells.
Fig. S4 (IAI00002-23-s0004.tif). Pro-Caspase transcript levels increase during *E. chaffeensis* infection.

REFERENCES

1. Jaworski DC, Cheng C, Nair ADS, Ganta RR. 2017. *Amblyomma americanum* ticks infected with *in vitro* cultured wild-type and mutants of *Ehrlichia chaffeensis* are competent to produce infection in naïve deer and dogs. Ticks Tick Borne Dis 8:60–64. https://doi.org/10.1016/j.ttbdis.2016.09.017
2. Byerly CD, Mitra S, Patterson LL, Pittner NA, Velayutham TS, Paessler S, Veljkovic V, McBride JW. 2022. *Ehrlichia* SLiM ligand mimetic activates Hedgehog signaling to engage a BCL-2 anti-apoptotic cellular program. PLoS Pathog 18:e1010345. https://doi.org/10.1371/journal.ppat.1010345
3. Byerly CD, Patterson LL, McBride JW. 2021. *Ehrlichia* TRP effectors: moonlighting, mimicry and infection. Pathog Dis 79:ftab026. https://doi.org/10.1093/femspd/ftab026
4. Klema VJ, Sepuru KM, Füllbrunn N, Farris TR, Dunphy PS, McBride JW, Rajarathnam K, Choi KH. 2018. *Ehrlichia chaffeensis* TRP120 nucleomodulin binds DNA with disordered tandem repeat domain. PLoS One 13:e0194891. https://doi.org/10.1371/journal.pone.0194891
5. Lina TT, Dunphy PS, Luo T, McBride JW. 2016. *Ehrlichia chaffeensis* TRP120 activates canonical notch signaling to downregulate TLR2/4 expression and promote intracellular survival. mBio 7:e00672-16. https://doi.org/10.1128/mBio.00672-16
6. Lina TT, Luo T, Velayutham T-S, Das S, McBride JW. 2017. *Ehrlichia* activation of Wnt-PI3K-mTOR signaling inhibits autolysosome generation and autophagic destruction by the mononuclear phagocyte. Infect Immun 85:e00690-17. https://doi.org/10.1128/IAI.00690-17
7. Luo T, Dunphy PS, Lina TT, McBride JW. 2015. *Ehrlichia chaffeensis* exploits canonical and noncanonical host Wnt signaling pathways to stimulate phagocytosis and promote intracellular survival. Infect Immun 84:686–700. https://doi.org/10.1128/IAI.01289-15
8. Luo T, Dunphy PS, McBride JW. 2017. *Ehrlichia chaffeensis* tandem repeat effector targets differentially influence infection. Front Cell Infect Microbiol 7:178. https://doi.org/10.3389/fcimb.2017.00178
9. Luo T, Kuriakose JA, Zhu B, Wakeel A, McBride JW. 2011. *Ehrlichia chaffeensis* TRP120 interacts with a diverse array of eukaryotic proteins involved in transcription, signaling, and cytoskeleton organization. Infect Immun 79:4382–4391. https://doi.org/10.1128/IAI.05608-11
10. Luo T, McBride JW. 2012. *Ehrlichia chaffeensis* TRP32 interacts with host cell targets that influence intracellular survival. Infect Immun 80:2297–2306. https://doi.org/10.1128/IAI.00154-12
11. Luo T, Mitra S, McBride JW, D'Orazio SEF. 2018. *Ehrlichia chaffeensis* TRP75 interacts with host cell targets involved in homeostasis, cytoskeleton organization, and apoptosis regulation to promote infection. mSphere 3:e00147-18. https://doi.org/10.1128/mSphere.00147-18
12. Mitra S, Dunphy PS, Das S, Zhu B, Luo T, McBride JW. 2018. *Ehrlichia chaffeensis* TRP120 effector targets and recruits host polycomb group proteins for degradation to promote intracellular infection. Infect Immun 86:e00845-17. https://doi.org/10.1128/IAI.00845-17
13. Patterson LL, Velayutham TS, Byerly CD, Bui DC, Patel J, Veljkovic V, Paessler S, McBride JW, Carlyon JA, Norris SJ. 2022. *Ehrlichia* SLiM ligand mimetic activates Notch signaling in human monocytes. mBio 13:e0007622. https://doi.org/10.1128/mbio.00076-22
14. Rogan MR, Patterson LL, Byerly CD, Luo T, Paessler S, Veljkovic V, Quade B, McBride JW. 2021. *Ehrlichia chaffeensis* TRP120 is a Wnt ligand mimetic that interacts with Wnt receptors and contains a novel repetitive short linear motif that activates Wnt signaling. mSphere 6:e00216-21. https://doi.org/10.1128/mSphere.00216-21
15. Wang JY, Zhu B, Patterson LL, Rogan MR, Kibler CE, McBride JW. 2020. *Ehrlichia chaffeensis* TRP120-mediated ubiquitination and proteasomal degradation of tumor suppressor FBW7 increases oncoprotein stability and promotes infection. PLoS Pathog 16:e1008541. https://doi.org/10.1371/journal.ppat.1008541
16. Zhu B, Das S, Mitra S, Farris TR, McBride JW. 2017. *Ehrlichia chaffeensis* TRP120 moonlights as a HECT E3 Ligase involved in self- and host ubiquitination to influence protein interactions and stability for intracellular survival. Infect Immun 85:e00290-17. https://doi.org/10.1128/IAI.00290-17
17. Zhu B, Farris TR, Milligan HS, Chen HS, Zhu RJ, Hong AL, Zhou XC, Gao XL. 2015. Analysis of *Ehrlichia Chaffeensis* Multifunctional Trp120 Effector Ubiquitinylation by Microfluidic peptide array, Abstr American Society of Microbiology Annual Meeting;
18. Zhu B, Kuriakose JA, Luo T, Ballesteros E, Gupta S, Fofanov Y, McBride JW. 2011. *Ehrlichia chaffeensis* TRP120 binds a G+C-rich motif in host cell DNA and exhibits eukaryotic transcriptional activator function. Infect Immun 79:4370–4381. https://doi.org/10.1128/IAI.05422-11
19. Luo T, Patel JG, Zhang X, Walker DH, McBride JW. 2020. *Ehrlichia chaffeensis* and *E. canis* hypothetical protein immunoanalysis reveals small secreted immunodominant proteins and conformation-dependent antibody epitopes. NPJ Vaccines 5:85. https://doi.org/10.1038/s41541-020-00231-1
20. Kuriakose JA, Zhang X, Luo T, McBride JW. 2012. Molecular basis of antibody mediated immunity against *Ehrlichia chaffeensis* involves

species-specific linear epitopes in tandem repeat proteins. Microbes Infect 14:1054–1063. https://doi.org/10.1016/j.micinf.2012.05.012
21. McBride JW, Comer JE, Walker DH. 2003. Novel immunoreactive glycoprotein orthologs of *Ehrlichia* spp. Ann N Y Acad Sci 990:678–684. https://doi.org/10.1111/j.1749-6632.2003.tb07443.x
22. McBride JW, Corstvet RE, Gaunt SD, Boudreaux C, Guedry T, Walker DH. 2003. Kinetics of antibody response to *Ehrlichia canis* immunoreactive proteins. Infect Immun 71:2516–2524. https://doi.org/10.1128/IAI.71.5.2516-2524.2003
23. Popov VL, Yu X j, Walker DH. 2000. The 120 kDa outer membrane protein of *Ehrlichia chaffeensis*: preferential expression on dense-core cells and gene expression in *Escherichia coli* associated with attachment and entry. Microb Pathog 28:71–80. https://doi.org/10.1006/mpat.1999.0327
24. Dunphy PS, Luo T, McBride JW. 2014. *Ehrlichia chaffeensis* exploits host SUMOylation pathways to mediate effector-host interactions and promote intracellular survival. Infect Immun 82:4154–4168. https://doi.org/10.1128/IAI.01984-14
25. Liu H, Bao W, Lin M, Niu H, Rikihisa Y. 2012. Ehrlichia type IV secretion effector ECH0825 is translocated to mitochondria and curbs ROS and apoptosis by upregulating host MnSOD. Cell Microbiol 14:1037–1050. https://doi.org/10.1111/j.1462-5822.2012.01775.x
26. Beaudouin J, Liesche C, Aschenbrenner S, Hörner M, Eils R. 2013. Caspase-8 cleaves its substrates from the plasma membrane upon CD95-induced apoptosis. Cell Death Differ 20:599–610. https://doi.org/10.1038/cdd.2012.156
27. Fu T-M, Li Y, Lu A, Li Z, Vajjhala PR, Cruz AC, Srivastava DB, DiMaio F, Penczek PA, Siegel RM, Stacey KJ, Egelman EH, Wu H. 2016. Cryo-EM structure of caspase-8 tandem DED filament reveals assembly and regulation mechanisms of the death-inducing signaling complex. Mol Cell 64:236–250. https://doi.org/10.1016/j.molcel.2016.09.009
28. Hughes MA, Powley IR, Jukes-Jones R, Horn S, Feoktistova M, Fairall L, Schwabe JWR, Leverkus M, Cain K, MacFarlane M. 2016. Co-operative and hierarchical binding of C-FLIP and Caspase-8: a unified model defines how c-FLIP isoforms differentially control cell fate. Mol Cell 61:834–849. https://doi.org/10.1016/j.molcel.2016.02.023
29. Brentnall M, Rodriguez-Menocal L, De Guevara RL, Cepero E, Boise LH. 2013. Caspase-9, caspase-3 and caspase-7 have distinct roles during intrinsic apoptosis. BMC Cell Biol 14:32. https://doi.org/10.1186/1471-2121-14-32
30. Bock FJ, Tait SWG. 2020. Mitochondria as multifaceted regulators of cell death. Nat Rev Mol Cell Biol 21:85–100. https://doi.org/10.1038/s41580-019-0173-8
31. Abe Y, Oda-Sato E, Tobiume K, Kawauchi K, Taya Y, Okamoto K, Oren M, Tanaka N. 2008. Hedgehog signaling overrides p53-mediated tumor suppression by activating Mdm2. Proc Natl Acad Sci U S A 105:4838–4843. https://doi.org/10.1073/pnas.0712216105
32. Elmore S. 2007. Apoptosis: a review of programmed cell death. Toxicol Pathol 35:495–516. https://doi.org/10.1080/01926230701320337
33. Zhang J, Sinha M, Luxon BA, Yu X. 2004. Survival strategy of obligately intracellular *Ehrlichia chaffeensis*: novel modulation of immune response and host cell cycles. Infect Immun 72:498–507. https://doi.org/10.1128/IAI.72.1.498-507.2004
34. Palaga T, Buranaruk C, Rengpipat S, Fauq AH, Golde TE, Kaufmann SHE, Osborne BA. 2008. Notch signaling is activated by TLR stimulation and regulates macrophage functions. Eur J Immunol 38:174–183. https://doi.org/10.1002/eji.200636999
35. Palaga T, Ratanabunyong S, Pattarakankul T, Sangphech N, Wongchana W, Hadae Y, Kueanjinda P. 2013. Notch signaling regulates expression of Mcl-1 and apoptosis in PPD-treated macrophages. Cell Mol Immunol 10:444–452. https://doi.org/10.1038/cmi.2013.22
36. Shang Y, Smith S, Hu X. 2016. Role of Notch signaling in regulating innate immunity and inflammation in health and disease. Protein Cell 7:159–174. https://doi.org/10.1007/s13238-016-0250-0
37. Zhang Q, Wang C, Liu Z, Liu X, Han C, Cao X, Li N. 2012. Notch signal suppresses toll-like receptor-triggered inflammatory responses in macrophages by inhibiting extracellular signal-regulated kinase 1/2-mediated nuclear factor kappaB activation. J Biol Chem 287:6208–6217. https://doi.org/10.1074/jbc.M111.310375
38. Miele L, Osborne B. 1999. Arbiter of differentiation and death: Notch signaling meets apoptosis. J Cell Physiol 181:393–409. https://doi.org/10.1002/(SICI)1097-4652(199912)181:3<393::AID-JCP3>3.0.CO;2-6
39. Lin M, Rikihisa Y. 2004. *Ehrlichia chaffeensis* downregulates surface Toll-like receptors 2/4, CD14 and transcription factors PU.1 and inhibits lipopolysaccharide activation of NF-κB, ERK 1/2 and p38 MAPK in host monocytes. Cell Microbiol 6:175–186. https://doi.org/10.1046/j.1462-5822.2003.00355.x
40. Strasser A, O'Connor L, Dixit VM. 2000. Apoptosis signaling. Annu Rev Biochem 69:217–245. https://doi.org/10.1146/annurev.biochem.69.1.217
41. Lu M, Lin S-C, Huang Y, Kang YJ, Rich R, Lo Y-C, Myszka D, Han J, Wu H. 2007. XIAP induces NF-kappaB activation via the BIR1/TAB1 interaction and BIR1 dimerization. Mol Cell 26:689–702. https://doi.org/10.1016/j.molcel.2007.05.006
42. Suzuki Y, Nakabayashi Y, Takahashi R. 2001. Ubiquitin-protein ligase activity of X-linked inhibitor of apoptosis protein promotes proteasomal degradation of caspase-3 and enhances its anti-apoptotic effect in Fas-induced cell death. Proc Natl Acad Sci U S A 98:8662–8667. https://doi.org/10.1073/pnas.161506698
43. Ge Y, Rikihisa Y. 2006. *Anaplasma phagocytophilum* delays spontaneous human neutrophil apoptosis by modulation of multiple apoptotic pathways. Cell Microbiol 8:1406–1416. https://doi.org/10.1111/j.1462-5822.2006.00720.x
44. Riedl SJ, Renatus M, Schwarzenbacher R, Zhou Q, Sun C, Fesik SW, Liddington RC, Salvesen GS. 2001. Structural basis for the inhibition of caspase-3 by XIAP. Cell 104:791–800. https://doi.org/10.1016/s0092-8674(01)00274-4
45. Srinivasula SM, Hegde R, Saleh A, Datta P, Shiozaki E, Chai J, Lee RA, Robbins PD, Fernandes-Alnemri T, Shi Y, Alnemri ES. 2001. A conserved XIAP-interaction motif in caspase-9 and Smac/DIABLO regulates caspase activity and apoptosis. Nature 410:112–116. https://doi.org/10.1038/35065125
46. Sun C, Cai M, Meadows RP, Xu N, Gunasekera AH, Herrmann J, Wu JC, Fesik SW. 2000. NMR structure and mutagenesis of the third Bir domain of the inhibitor of apoptosis protein XIAP. J Biol Chem 275:33777–33781. https://doi.org/10.1074/jbc.M006226200
47. Liu W-H, Hsiao H-W, Tsou W-I, Lai M-Z. 2007. Notch inhibits apoptosis by direct interference with XIAP ubiquitination and degradation. EMBO J 26:1660–1669. https://doi.org/10.1038/sj.emboj.7601611
48. Deveraux QL, Leo E, Stennicke HR, Welsh K, Salvesen GS, Reed JC. 1999. Cleavage of human inhibitor of apoptosis protein XIAP results in fragments with distinct specificities for caspases. EMBO J 18:5242–5251. https://doi.org/10.1093/emboj/18.19.5242
49. Peterson QP, Goode DR, West DC, Botham RC, Hergenrother PJ. 2010. Preparation of the caspase-3/7 substrate Ac-DEVD-pNA by solution-phase peptide synthesis. Nat Protoc 5:294–302. https://doi.org/10.1038/nprot.2009.223
50. Creagh EM, Murphy BM, Duriez PJ, Duckett CS, Martin SJ. 2004. Smac/Diablo antagonizes ubiquitin ligase activity of inhibitor of apoptosis proteins. J Biol Chem 279:26906–26914. https://doi.org/10.1074/jbc.M313859200
51. Scott FL, Denault J-B, Riedl SJ, Shin H, Renatus M, Salvesen GS. 2005. XIAP inhibits caspase-3 and -7 using two binding sites: evolutionarily conserved mechanism of Iaps. EMBO J 24:645–655. https://doi.org/10.1038/sj.emboj.7600544
52. Liu Y, Zhang Z, Jiang Y, Zhang L, Popov VL, Zhang J, Walker DH, Yu X. 2011. Obligate intracellular bacterium *Ehrlichia* inhibiting mitochondrial activity. Microbes Infect 13:232–238. https://doi.org/10.1016/j.micinf.2010.10.021
53. Rikihisa Y. 2006. *Ehrlichia* subversion of host innate responses. Curr Opin Microbiol 9:95–101. https://doi.org/10.1016/j.mib.2005.12.003
54. Lin M, Liu H, Xiong Q, Niu H, Cheng Z, Yamamoto A, Rikihisa Y. 2016. *Ehrlichia* secretes Etf-1 to induce autophagy and capture nutrients for its growth through RAB5 and class III phosphatidylinositol 3-kinase. Autophagy 12:2145–2166. https://doi.org/10.1080/15548627.2016.1217369
55. Choi K-S, Webb T, Oelke M, Scorpio DG, Dumler JS. 2007. Differential innate immune cell activation and proinflammatory response in *Anaplasma phagocytophilum* infection. Infect Immun 75:3124–3130. https://doi.org/10.1128/IAI.00098-07
56. Fischer A, Harrison KS, Ramirez Y, Auer D, Chowdhury SR, Prusty BK, Sauer F, Dimond Z, Kisker C, Hefty PS, Rudel T. 2017. *Chlamydia trachomatis*-containing vacuole serves as deubiquitination platform to

stabilize Mcl-1 and to interfere with host defense. Elife 6:e21465. https://doi.org/10.7554/eLife.21465
57. Forsberg M, Blomgran R, Lerm M, Särndahl E, Sebti SM, Hamilton A, Stendahl O, Zheng L. 2003. Differential effects of invasion by and phagocytosis of *Salmonella typhimurium* on apoptosis in human macrophages: potential role of Rho–GTPases and Akt. J Leukoc Biol 74:620–629. https://doi.org/10.1189/jlb.1202586
58. Ge Y, Yoshiie K, Kuribayashi F, Lin M, Rikihisa Y. 2005. *Anaplasma phagocytophilum* inhibits human neutrophil apoptosis via upregulation of *bfl*-1, maintenance of mitochondrial membrane potential and prevention of caspase 3 activation. Cell Microbiol 7:29–38. https://doi.org/10.1111/j.1462-5822.2004.00427.x
59. Holla S, Ghorpade DS, Singh V, Bansal K, Balaji KN. 2014. *Mycobacterium bovis* BCG promotes tumor cell survival from tumor necrosis factor-α-induced apoptosis. Mol Cancer 13:210. https://doi.org/10.1186/1476-4598-13-210
60. Hueffer K, Galán JE. 2004. *Salmonella*-induced macrophage death: multiple mechanisms, different outcomes. Cell Microbiol 6:1019–1025. https://doi.org/10.1111/j.1462-5822.2004.00451.x
61. Chen F, Cheng W, Zhang S, Zhong G, Yu P. 2010. Induction of IL-8 by chlamydia trachomatis through MAPK pathway rather than NF-kappaB pathway. Zhong Nan Da Xue Xue Bao Yi Xue Ban 35:307–313. https://doi.org/10.3969/j.issn.1672-7347.2010.04.005
62. Choi K-S, Park JT, Dumler JS. 2005. *Anaplasma phagocytophilum* delay of neutrophil apoptosis through the P38 mitogen-activated protein kinase signal pathway. Infect Immun 73:8209–8218. https://doi.org/10.1128/IAI.73.12.8209-8218.2005
63. Figueiredo JF, Lawhon SD, Gokulan K, Khare S, Raffatellu M, Tsolis RM, Bäumler AJ, McCormick BA, Adams LG. 2009. *Salmonella enterica* typhimurium SipA induces CXC-chemokine expression through p38MAPK and JUN pathways. Microbes Infect 11:302–310. https://doi.org/10.1016/j.micinf.2008.12.005
64. Popa CM, Tabuchi M, Valls M. 2016. Modification of bacterial effector proteins inside eukaryotic host cells. Front Cell Infect Microbiol 6:73. https://doi.org/10.3389/fcimb.2016.00073
65. Balcewicz-Sablinska MK, Keane J, Kornfeld H, Remold HG. 1998. Pathogenic Mycobacterium tuberculosis evades apoptosis of host macrophages by release of TNF-R2, resulting in inactivation of TNF-alpha. J Immunol 161:2636–2641.
66. Bastidas RJ, Elwell CA, Engel JN, Valdivia RH. 2013. Chlamydial intracellular survival strategies. Cold Spring Harb Perspect Med 3:a010256. https://doi.org/10.1101/cshperspect.a010256
67. Artavanis-Tsakonas S. 1988. The molecular biology of the Notch locus and the fine tuning of differentiation in *Drosophila*. Trends Genet 4:95–100. https://doi.org/10.1016/0168-9525(88)90096-0
68. Artavanis-Tsakonas S, Rand MD, Lake RJ. 1999. Notch signaling: cell fate control and signal integration in development. Science 284:770–776. https://doi.org/10.1126/science.284.5415.770
69. Song B, Chi Y, Li X, Du W, Han Z-B, Tian J, Li J, Chen F, Wu H, Han L, Lu S, Zheng Y, Han Z. 2015. Inhibition of Notch signaling promotes the adipogenic differentiation of mesenchymal stem cells through autophagy activation and PTEN-PI3K/AKT/mTOR pathway. Cell Physiol Biochem 36:1991–2002. https://doi.org/10.1159/000430167
70. Andersen P, Uosaki H, Shenje LT, Kwon C. 2012. Non-canonical Notch signaling: emerging role and mechanism. Trends Cell Biol 22:257–265. https://doi.org/10.1016/j.tcb.2012.02.003
71. Palomero T, Sulis ML, Cortina M, Real PJ, Barnes K, Ciofani M, Caparros E, Buteau J, Brown K, Perkins SL, Bhagat G, Agarwal AM, Basso G, Castillo M, Nagase S, Cordon-Cardo C, Parsons R, Zúñiga-Pflücker JC, Dominguez M, Ferrando AA. 2007. Mutational loss of PTEN induces resistance to NOTCH1 inhibition in T-cell leukemia. Nat Med 13:1203–1210. https://doi.org/10.1038/nm1636
72. Radtke F, MacDonald HR, Tacchini-Cottier F. 2013. Regulation of innate and adaptive immunity by Notch. Nat Rev Immunol 13:427–437. https://doi.org/10.1038/nri3445
73. Zweidler-McKay PA, He Y, Xu L, Rodriguez CG, Karnell FG, Carpenter AC, Aster JC, Allman D, Pear WS. 2005. Notch signaling is a potent inducer of growth arrest and apoptosis in a wide range of B-cell malignancies. Blood 106:3898–3906. https://doi.org/10.1182/blood-2005-01-0355
74. Tsao P-N, Wei S-C, Huang M-T, Lee M-C, Chou H-C, Chen C-Y, Hsieh W-S. 2011. Lipopolysaccharide-induced Notch signaling activation through JNK-dependent pathway regulates inflammatory response. J Biomed Sci 18:56. https://doi.org/10.1186/1423-0127-18-56
75. Narayana Y, Balaji KN. 2008. Notch1 up-regulation and signaling involved in *Mycobacterium bovis* BCG-induced SOCS3 expression in macrophages. J Biol Chem 283:12501–12511. https://doi.org/10.1074/jbc.M709960200
76. Shiozaki EN, Chai J, Rigotti DJ, Riedl SJ, Li P, Srinivasula SM, Alnemri ES, Fairman R, Shi Y. 2003. Mechanism of XIAP-mediated inhibition of caspase-9. Mol Cell 11:519–527. https://doi.org/10.1016/s1097-2765(03)00054-6
77. Zhivotovsky B, Samali A, Gahm A, Orrenius S. 1999. Caspases: their intracellular localization and translocation during apoptosis. Cell Death Differ 6:644–651. https://doi.org/10.1038/sj.cdd.4400536
78. Delbue D, Mendonça BS, Robaina MC, Lemos LGT, Lucena PI, Viola JPB, Magalhães LM, Crocamo S, Oliveira CAB, Teixeira FR, Maia RC, Nestal de Moraes G. 2020. Expression of nuclear XIAP associates with cell growth and drug resistance and confers poor prognosis in breast cancer. Biochim Biophys Acta Mol Cell Res 1867:118761. https://doi.org/10.1016/j.bbamcr.2020.118761
79. Cao Z, Li X, Li J, Luo W, Huang C, Chen J. 2014. X-linked inhibitor of apoptosis protein (XIAP) lacking RING domain localizes to the nuclear and promotes cancer cell anchorage-independent growth by targeting the E2F1/Cyclin E axis. Oncotarget 5:7126–7137. https://doi.org/10.18632/oncotarget.2227
80. Xiao Y, Zhong Y, Greene W, Dong F, Zhong G. 2004. *Chlamydia trachomatis* infection inhibits both Bax and Bak activation induced by staurosporine. Infect Immun 72:5470–5474. https://doi.org/10.1128/IAI.72.9.5470-5474.2004
81. Banga S, Gao P, Shen X, Fiscus V, Zong W-X, Chen L, Luo Z-Q. 2007. *Legionella pneumophila* inhibits macrophage apoptosis by targeting pro-death members of the BCL2 protein family. Proc Natl Acad Sci U S A 104:5121–5126. https://doi.org/10.1073/pnas.0611030104
82. Alberdi P, Espinosa PJ, Cabezas-Cruz A, de la Fuente J. 2016. *Anaplasma phagocytophilum* manipulates host cell apoptosis by different mechanisms to establish infection. Vet Sci 3:15. https://doi.org/10.3390/vetsci3030015
83. Zhang J, Sinha M, Luxon BA, Yu X. 2004. Survival strategy of obligately intracellular *Ehrlichia chaffeensis*: novel modulation of immune response and host cell cycles. Infect Immun 72:498–507. https://doi.org/10.1128/IAI.72.1.498-507.2004
84. Hörnle M, Peters N, Thayaparasingham B, Vörsmann H, Kashkar H, Kulms D. 2011. Caspase-3 cleaves XIAP in a positive feedback loop to sensitize melanoma cells to TRAIL-induced apoptosis. Oncogene 30:575–587. https://doi.org/10.1038/onc.2010.434
85. Lu J, Bai L, Sun H, Nikolovska-Coleska Z, McEachern D, Qiu S, Miller RS, Yi H, Shangary S, Sun Y, Meagher JL, Stuckey JA, Wang S. 2008. SM-164: a novel, bivalent smac mimetic that induces apoptosis and tumor regression by concurrent removal of the blockade of cIAP-1/2 and XIAP. Cancer Res 68:9384–9393. https://doi.org/10.1158/0008-5472.CAN-08-2655
86. Wei MC, Lindsten T, Mootha VK, Weiler S, Gross A, Ashiya M, Thompson CB, Korsmeyer SJ. 2000. tBID, a membrane-targeted death ligand, oligomerizes BAK to release cytochrome c. Genes Dev 14:2060–2071.
87. Wu M-S, Wang G-F, Zhao Z-Q, Liang Y, Wang H-B, Wu M-Y, Min P, Chen L, Feng Q-S, Bei J-X, Zeng Y-X, Yang D. 2013. Smac mimetics in combination with TRAIL selectively target cancer stem cells in nasopharyngeal carcinoma. Mol Cancer Ther 12:1728–1737. https://doi.org/10.1158/1535-7163.MCT-13-0017
88. Matsumoto A, Onoyama I, Sunabori T, Kageyama R, Okano H, Nakayama KI. 2011. Fbxw7-dependent degradation of Notch is required for control of "Stemness" and neuronal-glial differentiation in neural stem cells. J Biol Chem 286:13754–13764. https://doi.org/10.1074/jbc.M110.194936
89. Rajalingam K, Sharma M, Paland N, Hurwitz R, Thieck O, Oswald M, Machuy N, Rudel T, Galan J. 2006. IAP-IAP complexes required for apoptosis resistance of *C. trachomatis*-infected cells. PLoS Pathog 2:e114. https://doi.org/10.1371/journal.ppat.0020114
90. Tasca A, Helmstädter M, Brislinger MM, Haas M, Mitchell B, Walentek P. 2021. Notch signaling induces either apoptosis or cell fate change in multiciliated cells during mucociliary tissue remodeling. Dev Cell 56:525–539. https://doi.org/10.1016/j.devcel.2020.12.005

91. Lu J, Wang D, Shen J. 2017. Hedgehog signalling is required for cell survival in *Drosophila* wing pouch cells. Sci Rep 7:11317. https://doi.org/10.1038/s41598-017-10550-4
92. Velayutham TS, Kumar S, Zhang X, Kose N, Walker DH, Winslow G, Crowe JE, McBride JW. 2019. *Ehrlichia chaffeensis* outer membrane protein 1-specific human antibody-mediated immunity is defined by intracellular TRIM21-dependent innate immune activation and extracellular neutralization. Infect Immun 87:e00383-19. https://doi.org/10.1128/IAI.00383-19
93. Luo T, Zhang X, McBride JW. 2009. Major species-specific antibody epitopes of the *Ehrlichia chaffeensis* p120 and *E. canis* p140 orthologs in surface-exposed tandem repeat regions. Clin Vaccine Immunol 16:982–990. https://doi.org/10.1128/CVI.00048-09
94. Doyle CK, Nethery KA, Popov VL, McBride JW. 2006. Differentially expressed and secreted major immunoreactive protein orthologs of *Ehrlichia canis* and *E. chaffeensis* elicit early antibody responses to epitopes on glycosylated tandem repeats. Infect Immun 74:711–720. https://doi.org/10.1128/IAI.74.1.711-720.2006
95. Luo T, Zhang X, Wakeel A, Popov VL, McBride JW. 2008. A variable-length PCR target protein of *Ehrlichia chaffeensis* contains major species-specific antibody epitopes in acidic serine-rich tandem repeats. Infect Immun 76:1572–1580. https://doi.org/10.1128/IAI.01466-07